USGS
science for a changing world

Questa Baseline and Premining Ground-Water Quality Investigation 10.

Geologic Influences on Ground and Surface Waters in the Red River Watershed, New Mexico

Scientific Investigations Report 2004-5245

U.S. Department of the Interior
U.S. Geological Survey

Questa Baseline and Premining Ground-Water Quality Investigation 10.

Geologic Influences on Ground and Surface Waters in the Red River Watershed, New Mexico

By Steve Ludington, Geoff Plumlee, Jonathan Caine,
Dana Bove, JoAnn Holloway, and Eric Livo

Prepared in cooperation with the New Mexico Environment Department

Scientific Investigations Report 2004-5245

U.S. Department of the Interior
U.S. Geological Survey

U.S. Department of the Interior
Gale A. Norton, Secretary

U.S. Geological Survey
P. Patrick Leahy, Acting Director

U.S. Geological Survey, Reston, Virginia: 2005

For product and ordering information:
World Wide Web: http://www.usgs.gov/pubprod/
Telephone: 1-888-ASK-USGS

For more information on the USGS—the Federal source for science about the Earth,
its natural and living resources, natural hazards, and the environment:
World Wide Web: http://www.usgs.gov/
Telephone: 1-888-ASK-USGS

Suggested citation:
Ludington, Steve, Plumlee, Geoff, Caine, Jonathan, Bove, Dana, Holloway, JoAnne, and Livo, Eric, 2005, Questa baseline and premining ground-water quality investigation 10—Geologic influences on ground and surface waters in the Red River watershed, New Mexico: U.S. Geological Survey Scientific Investigations Report 2004-5245, 41 p.

Contents

Introduction....1
Methods Used in this Study....3
Geologic Setting....3
Mineralization and Alteration....3
Alteration in Climax-Type Deposits....7
Alteration at Questa....7
District-Wide Alteration Zoning....9
District-Wide Geochemical Patterns at Questa....9
Geology and Alteration of Red River Alteration Scars....15
Bedrock Geology....17
Spatial Variations in Hypogene Mineralization and Alteration Between Scar Areas....23
Variable Erosion Levels within Mineralized Intrusive Centers along the Lower Red River....26
Oxidation, Weathering, and Erosion Processes Active in Scars....26
Mineralogic Variations in a Weathered Profile Developed on QSP-Altered and Propylitically Altered Andesite....26
Chemical and Physical Weathering Mechanisms in Rocks Affected by QSP Alteration....30
Weathering and Erosion of Amalia Tuff Altered to Advanced Argillic Assemblages....30
Relative Weathering Rates of Various Rock-Forming, Alteration, and Vein Minerals....32
Physical Slumping, Erosion Processes, and the Role of Soluble Secondary Salts....32
Characteristics of Materials in Debris Fans at the Base of Scar Areas....32
How Fast Do Mineralized Rocks in Scars Weather and Degrade?....33
Influences of Hydrothermal Mineralization-Alteration and Secondary Weathering on Ground- and Surface-Water Quality in the Red River Watershed....33
Geologic Structures and Bedrock Ground-Water Flow System....34
Are Unmined Erosional Scars Good Analogs for Mine-Site Scars under Premining Conditions?....37
Similarities Between Scar Areas....38
Differences Between Scar Areas....38
Summary....39
References....39

Figures

1. Index map of study area....1
2. Topographic map of study area showing erosional scars, debris fans, mineral deposits, and the Molycorp open pit....2
3. Generalized geologic map of the field area....4
4. Schematic cross section along profile A-A'....6
5. Map showing relative intensity of sericite alteration based on AVIRIS mapping....8

6. Cross sections showing inferred schematic spatial distributions of rock types, hydrothermal alteration types, and scar-area erosion levels around an idealized intrusion/mineralization center at Questa 10
7. Hand sample and transmitted-light photographs of thin sections showing progressive alteration of andesite, quartz latite porphyry, and Amalia Tuff....12
8. Photographs of mine bench on the upper west wall of Molycorp open pit and stockwork fractures in QSP-altered andesite, Straight Creek scar....15
9. Photographs of late-stage carbonate and (or) fluorite veining from the Molycorp open pit and various scar areas....16
10. Photomicrographs showing minerals from vein in QSP-altered and propylitically altered quartz latite porphyry, vein in QSP-altered Amalia Tuff, QSP-altered and propylitically altered andesite, and QSP-altered and propylitically altered quartz latite 17
11. Photographs showing occurrences of advanced argillic alteration associated with breccias, lower Red River valley....24
12. Satellite image of the lower Red River showing scar areas, Molycorp mine site, and the town of Red River 25
13. Photographs of weathering profile developed on QSP-altered and propylitically altered andesite, Straight Creek scar 27
14. Plots showing variations in the amounts of minerals across the Straight Creek scar weathering profile shown in figure 13....29
15. Photographs of house-size slump block of propylitized andesite sitting in shear contact on top of weathered, QSP-altered andesite within upper portions of the Sulphur Gulch scar....31
16. Photographs of decomposing pyrite-rich rock on debris fan extending from upper Sulphur Gulch scar onto uppermost bench of Molycorp open pit....33
17. Schematic west-to-east cross section of shallow subsurface at base of a typical scar area superimposed on photograph of the Hansen scar 35
18. Simplified geologic map of the Questa caldera 36
19. Fifteen-meter natural-color satellite image of study area draped on a USGS digital elevation model....37

Tables

1. Key characteristics of Red River scar areas, most sampled as part of this study....18
2. Quantitative X-ray diffraction results on selected hand samples or drill cutting samples showing how major mineralogy varies as a function of rock type, alteration type, and scar area 20
3. X-ray diffraction results on bulk samples and the < 2-mm fraction of samples collected from progressively higher elevations in a weathering profile, Straight Creek scar area....28

Geologic Influences on Ground and Surface Waters in the Red River Watershed, New Mexico

By Steve Ludington, Geoff Plumlee, Jonathan Caine, Dana Bove, JoAnn Holloway, and Eric Livo

Introduction

This report is one in a series that presents results of an interdisciplinary U.S. Geological Survey (USGS) study of ground-water quality in the lower Red River watershed prior to open-pit and underground molybdenite mining at Molycorp's Questa mine. The stretch of the Red River watershed that extends from just upstream of the town of Red River, N. Mex., to just above the town of Questa (fig. 1) includes several mineralized areas in addition to the one mined by Molycorp. Natural erosion and weathering of pyrite-rich rocks in the mineralized areas has created a series of erosional scars along this stretch of the Red River that contribute acidic waters, as well as mineralized alluvial material and sediments, to the river (fig. 2). The overall goal of the USGS study is to infer the premining ground-water quality at the Molycorp mine site. An integrated geologic, hydrologic, and geochemical model for ground water in the mineralized—but unmined—Straight Creek drainage (a tributary of the Red River) is being used as an analog for the geologic, geochemical, and hydrologic conditions that influenced ground-water quality and quantity in the Red River drainage prior to mining.

This report provides an overall geologic framework for the Red River watershed between Red River and Questa, in northern New Mexico, and summarizes key geologic, mineralogic, structural and other characteristics of various mineralized areas (and their associated erosional scars and debris fans) that likely influence ground- and surface-water quality and hydrology. The premining nature of the Sulphur Gulch and Goat Hill Gulch scars on the Molycorp mine site can be inferred through geologic comparisons with other unmined scars in the Red River drainage.

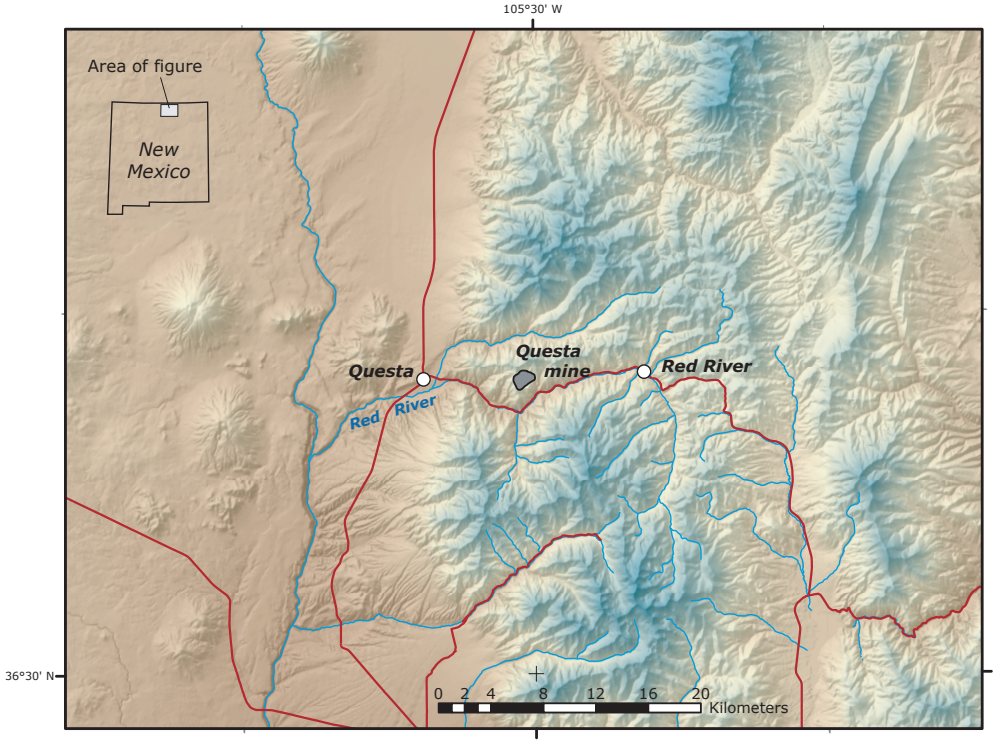

Figure 1. Index map of study area.

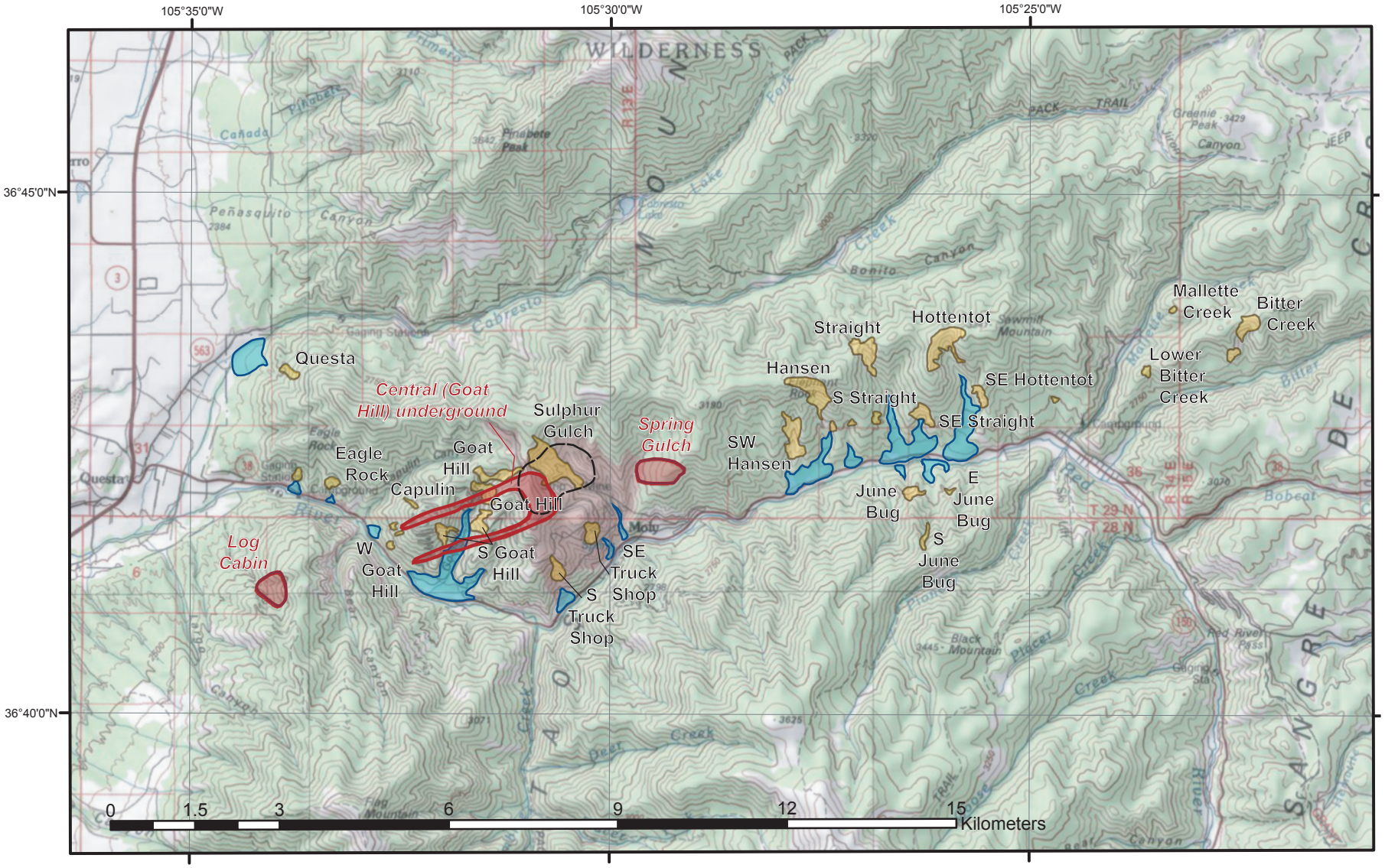

Figure 2. Topographic map of study area showing erosional scars (yellow), debris fans (light blue), ore bodies (red), and the Molycorp Questa mine (black dashed line).

A photographic overview of the chemical and physical weathering processes active in the alteration scars is presented by Plumlee, Ludington, and others (2005). Livo and Clark (2002) summarize results of an airborne visible-infrared imaging spectrometer (AVIRIS) remote-sensing study and presented maps showing the surface distribution of different hydrothermal minerals in the Red River watershed. Smith and others (2005) summarize the results of leach tests of surface material from the alteration scars and mine dumps—these materials inhibit the release of metals from mineralized rocks during snowmelt and rainfall. Caine (2003; written commun., 2004) presents field measurements of brittle structures and their potential impacts on the ground-water flow system in the lower Red River watershed.

Methods Used in this Study

This study includes a review of the literature, field sampling and observations, and mineralogical and chemical characterization of (1) bedrock outcrop samples from most of the scar areas and (2) drill cuttings from the USGS SC-1, SC-3, and SC-5 ground-water wells. Mineralogical characterization of most samples included semiquantitative X-ray diffraction (XRD), and a subset of key samples were characterized using quantitative XRD. Polished thin sections of a subset of the samples collected were also examined, and scanning electron microscopy (SEM) was used on a limited number of samples.

Geologic Setting

The Questa mine lies along the southern margin of the Questa caldera, which is part of the late Oligocene Latir volcanic field. The Latir volcanic field covers about 1,200 km^2 in north-central New Mexico and consists primarily of mildly alkaline rocks of intermediate composition that range from basaltic andesite volcanic and volcaniclastic rocks to peralkaline rhyolite flows and ash-flow tuffs. The volcanic rocks overlie Proterozoic crystalline basement that consists of metasedimentary and metavolcanic rocks that are intruded by granitic plutons. The volcanism culminated in the eruption of the mildly alkaline, rhyolitic Amalia Tuff and formation of the Questa caldera at about 25.7 Ma (Lipman, 1983; Lipman and Reed, 1989; Johnson and Lipman, 1988; Czamanske and others, 1990).

After formation of the Questa caldera, the volcanic rocks were subsequently intruded by a series of highly evolved high-silica granites and subvolcanic porphyries that are the apparent sources of hydrothermal fluids that formed a series of molybdenite deposits in the area. These granites and porphyries were emplaced after 25 Ma and occur as dikes and small stocks along a N. 75° E. trend that extends about 20 km from the Bear Canyon pluton, at the western range front, to at least the upper reaches of Bitter Creek, northeast of the village of Red River, N. Mex. (figs. 2 and 3). A second group of petrologically similar porphyries that are as young as 18 Ma was emplaced along a NW.-SE. trend from Bear Canyon pluton southward about 20 km to the vicinity of the Lucero Peak pluton (Ludington, 1981; Jones and Norris, 1984; Jones, 1990; Czamanske and others, 1990). It has been inferred by several workers (Martineau and others, 1977; Leonardson and others, 1983; Czamanske and others, 1990; Meyer, 1991; Lipman, 1992) that an elongate granitic batholith occurs at depth beneath the N. 75° E. trend and that it served as the parent body to the high-level stocks that gave rise to known mineral deposits along the lower Red River watershed (fig. 4). The postcaldera intrusions are structurally aligned with, but are younger than, the southern structural margin of the Questa caldera. The great composite thickness of dikes in both trends suggests first N.-S. extension, and later NE.-SW. extension, in the region.

The postcaldera intrusions are petrologically distinct from the caldera rocks. The silicic rocks of the caldera cycle are strongly alkaline (some are peralkaline) and are enriched in Y, Zr, and rare earth elements (REE). Younger mineralization-related intrusions are calc-alkaline, high in fluorine and silica, and strongly depleted in Y, Zr, and heavy REE, similar to the source rocks of other Climax-type molybdenite deposits (see Dillet and Czamanske, 1987; Johnson and others, 1989).

Mineralization and Alteration

Detailed descriptions of the molybdenite ores mined to date at Questa have been presented by Schilling (1956), Carpenter (1968), Leonardson and others (1983), Molling (1989), Meyer and Leonardson (1990), and Ross and others (2002). All of the mining to date has been from a horseshoe-shaped system of orebodies beneath Sulphur Gulch, Goat Hill, and Goat Hill Gulch. Separate constituents of this mineralized zone include veins of the original underground mine, mined during 1919–58; the material mined from the open pit during 1965–83; the Goat Hill orebody, mined by block caving during 1983–2000; and remaining reserves termed “D,” “Vein,” “Southwest Extension,” and “F-2” orebodies (Ross and others, 2002). Substantive mineralization has also been delineated to the west of the Questa mine in the Log Cabin orebody (on the upper contact of the Bear Canyon stock), and east of the Questa mine in the Spring Gulch orebody (figs. 2 and 4). Some exploration drilling was done in most of the alteration scars to the east of the mine, with the greatest focus on the Hottentot area (Loucks and others, 1977). Molybdenite mineralization was encountered, but no orebodies of sufficiently high grade to be considered economic were found.

The Questa deposits are considered to be Climax-type deposits, characterized by their genetic association with highly evolved, silica- and fluorine-rich rhyolite porphyry and granitic intrusive rocks. The ore deposits formed from magmatic-hydrothermal fluids that were expelled from magma as it crystallized to form the intrusive rocks. The

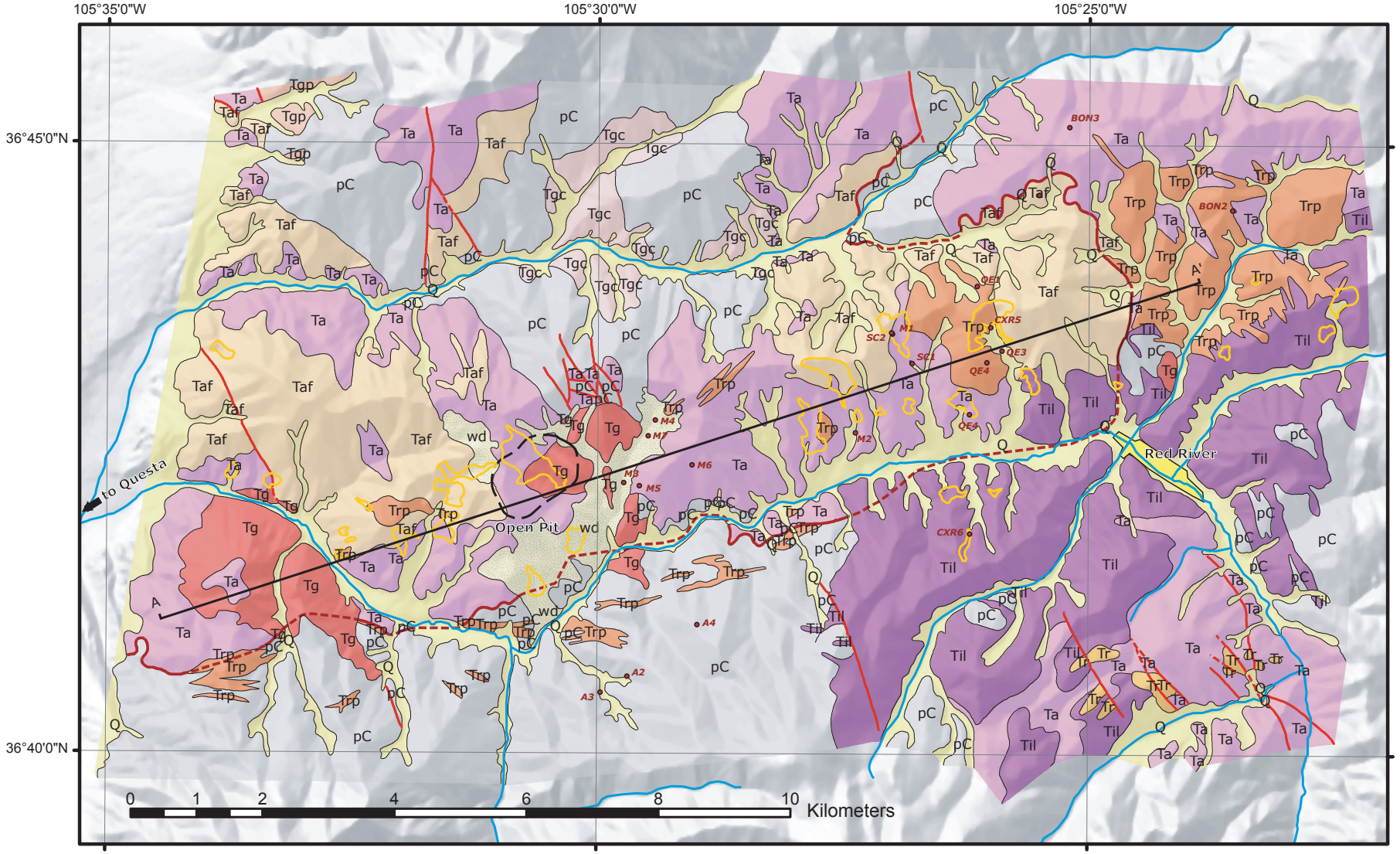

Scale 1:100,000. Map projection is UTM, zone 13N
Geographic coordinate system is North American datum of 1927

Figure 3. Generalized geologic map of the field area. Modified from Lipman and Reed (1989). See explanation on next page.

MAP EXPLANATION

wd—Mine waste dumps adjacent to the inactive open pit of the Questa molybdenum mine, consists of angular blocks and finer debris, primarily from the Sulphur Gulch pluton.

Q—Quaternary surficial deposits, primarily river alluvium, but includes colluvium, talus, landslide, and moraine deposits.

Tg—Medium- to fine-grained biotite granite, locally grading into aplite and aplite porphyry. SiO_2 commonly >76 percent. These plutons are postcaldera in age (24 to 25 Ma) and are related to molybdenite mineralization.

Tgc—Cabresto Lake pluton. Equigranular biotite-hornblende granite. SiO_2 is about 72 percent. Postcaldera in age, but unrelated to mineralization.

Tgp—Cañada Pinabete pluton. Fine-grained porphyritic biotite granite and aplite. Postcaldera in age, but unrelated to mineralization.

Trp—Porphyritic rhyolite. Rhyolite (74 to 77 percent SiO_2) with phenocrysts of quartz, sanidine, and sparse plagioclase and biotite. Occurs primarily as dikes and irregular masses, and forms the majority of the dikes in the swarm that trends N. 75° E. along the southern margin of the Questa caldera. Some bodies are transitional into porphyritic granite. Age ranges widely, and some may be contemporaneous with Tg and be related to molybdenite mineralization.

Til—Intrusive quartz latite. Porphyritic quartz latite, containing variable amounts of plagioclase, biotite, augite, hornblende, quartz, and sanidine. Occurs as large irregular laccolithic masses.

Tr—Rhyolitic lava flows. Flow-laminated alkali rhyolite with phenocrusts of quartz and alkali feldspar. Similar in composition to Amalia Tuff and peralkaline rhyolitic intrusions within the Questa caldera.

Taf—Amalia Tuff. Weakly to densely welded silicic alkalic ash-flow tuff. Commonly with SiO_2 > 77 percent. Fills Questa caldera to depths of at least 2 km. Age is late Oligocene, about 25.7 Ma.

Ta—Andesitic lava flows. Variable composition and color; texture ranging from porphyritic to aphanitic. Much propylitic alteration; boundaries between flows commonly obscure; also occurs as megabreccia blocks within caldera-filling ash-flow tuff.

pC—Proterozoic metamorphic and plutonic rocks.

CXR5 Drill hole, with label

Outline of alteration scar

Fault, dashed where concealed

Caldera wall, dashed where concealed

Geologic contact

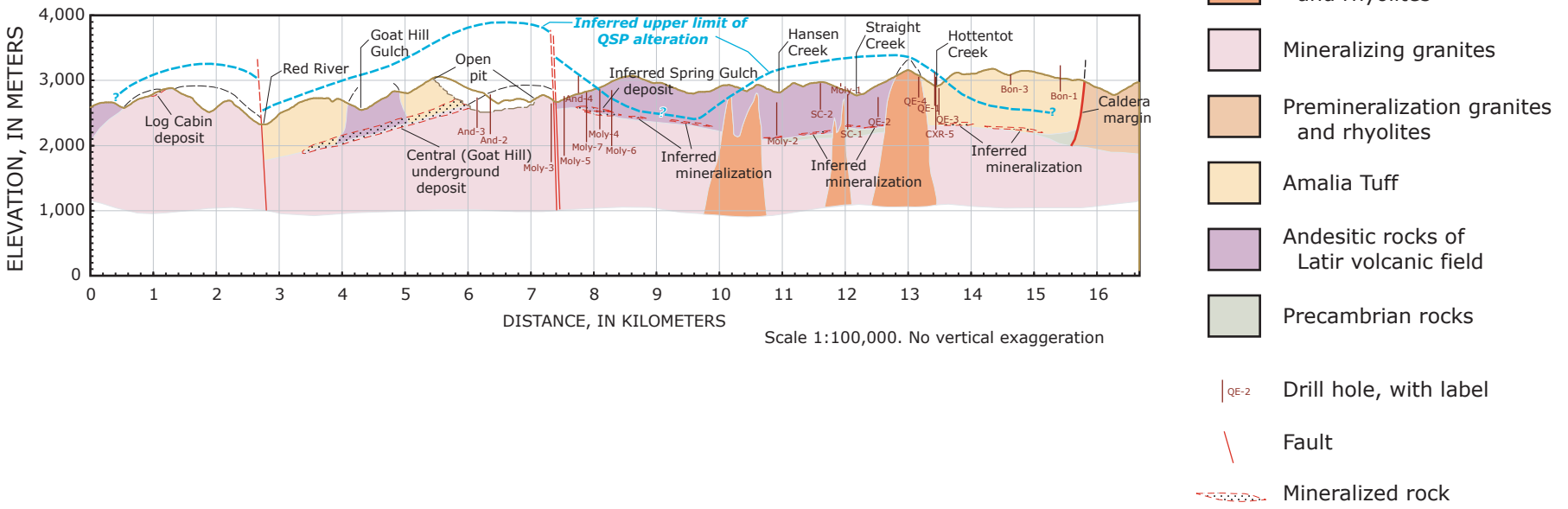

Figure 4. Schematic cross section along profile A-A′ (fig. 3), looking north. View is parallel to the N. 75° E. trend of dikes, stocks, and molybdenite mineralization discussed in the text. Exploration drill holes used for control of this interpretive section are projected to the plane of the section and labeled. Drill-hole data from Loucks and others (1977) and from other unpublished information on file at Molycorp mine offices. The inferred upper limit of QSP alteration is interpretive because there are few well-constrained control points on the ground.

magmatic-hydrothermal fluids deposited quartz, molybdenite, pyrite, fluorite, carbonates (primarily calcite, manganiferous calcite, dolomite, and rhodochrosite), and associated minerals in veins, stockwork vein systems, and breccia orebodies (Ross and others, 2002).

Hydrothermal alteration related to mineralizing processes can be found along the entire length of the N. 75° E. trend along the lower Red River valley, an area about 18 km long and at least 4 km wide (fig. 5). The nature of the alteration assemblages exposed at the surface is affected by many factors, among them the intensity of the underlying mineralization, the exposed rock type, and the amount of host-rock cover over the mineralized rock. A variety of geologic information has been integrated to indicate that the alteration and mineralization along the N. 75° E. trend is associated with a series of intrusions emplaced along the trend that are inferred to be of the same general age and composition.

Alteration in Climax-Type Deposits

Alteration and mineralization zoning patterns in Climax-type deposits provide a useful context in which to interpret the alteration and mineralization in the Questa mine and Red River scar areas. General discussions can be found in Westra and Keith (1981), Mutschler and others (1981), Ludington (1986), Carten and others (1993), and Ludington and others (1995). A central zone of fluorine-rich potassic alteration overlaps with and extends outward from the source intrusions responsible for mineralization. Potassic alteration is generally coincident with molybdenite mineralization and is typically succeeded upward (primarily) and outward by phyllic or quartz-sericite[1]-pyrite (QSP) alteration and, finally, by propylitic alteration. The total sulfide content (including molybdenite) of rocks from the potassic zone is commonly less than 3 weight percent, whereas the sulfide content of QSP zone rocks is much higher and may reach 10 weight percent or more (almost all as pyrite) (Westra and Keith, 1981). A zone of magnetite-hematite alteration and stockwork magnetite-hematite quartz veining may be locally developed between the outermost potassic and innermost QSP zones. Veins of primary gypsum or anhydrite may be present on the periphery of the potassic zone. Depending on original rock type, there may be sporadic development of an argillic alteration zone upward from the QSP zone. There is also a postmineralization overprint of carbonate-fluorite veinlets throughout much of the potassic and QSP zones.

Alteration at Questa

Our observations, coupled with those made in previous studies of the open-pit and underground orebodies at Questa (Martineau and others, 1977; Meyer and Leonardson, 1990; Ross and others, 2002) and exploration studies of the scar areas east of Questa (Loucks and others, 1977), indicate that the zoning of alteration assemblages around mineralizing intrusions at Questa (fig. 6) is generally similar to alteration zoning at other Climax-type deposits. Alteration associated directly with molybdenite mineralization is generally potassic, in which rocks, regardless of their type or composition, have been altered to a mixture of biotite, potassium feldspar, quartz, fluorite, and molybdenite. Potassic alteration at the Questa mine and in other Climax-type deposits is generally stronger and more pervasive than in other types of porphyry molybdenite deposits or in porphyry copper deposits.

Stockwork magnetite-hematite veining occurs in a shell overlapping the outer portions of the potassic zone in the Molycorp open pit, and primary hydrothermal anhydrite with intergrown secondary gypsum occurs in stockworks around the periphery of potassically altered rocks (Martineau and others, 1977). Similarly, limited occurrences of primary anhydrite/gypsum are also noted in drill core from beneath the Hansen, Straight, and Hottentot scar areas (Loucks and others, 1977).

Above the potassic alteration and known mineralized rocks, QSP, or phyllic, alteration is generally encountered. As the name implies, the rocks are altered to a mixture of quartz, pyrite, and sericite (fig. 7). In addition, QSP-altered rocks are crosscut by a complex network of intersecting veinlets as wide as 1 cm—these are called stockwork veinlets (figs. 7 and 8). Quartz and pyrite are the dominant veinlet-filling minerals and were deposited directly from hydrothermal fluids.

At Questa, the most pyrite-rich QSP alteration occurs in the andesite volcanic rocks and apparently resulted from the reaction of abundant iron-bearing silicates and iron-titanium oxides with sulfur-rich hydrothermal fluids. In contrast, in more silicic host rocks such as the rhyolite porphyries and the Amalia Tuff, QSP alteration is best developed only in areas relatively close to the source intrusions for mineralization. With increasing distance away from the source intrusions in these silicic rock types, the amount of hydrothermal pyrite decreases substantially, to the point where alteration is predominantly quartz-sericite (QS) with less than 1 percent total pyrite. This decrease likely reflects the substantially lower amounts of iron-bearing minerals in the silicic rocks available to react with hydrothermal sulfur.

In the mined orebodies at Questa, chalcopyrite and galena veins are noted to occur in a zone within the QSP zone (Martineau and others, 1977). To date, we have observed a galena-sphalerite-quartz vein only in one sample of drill core from beneath the Hottentot scar area.

In the mined orebodies, veins—usually late-stage—containing manganiferous calcite, dolomite, and fluorite occur spatially between but overlap both the molybdenite-bearing potassic alteration and the higher level QSP alteration (Ross and others, 2002; Martineau and others, 1977) (figs. 6, 9). We have found that carbonate minerals—usually microscopic—are commonly present in veins and disseminations in QSP-altered rocks in all of the mineralized areas. We have also observed possibly late-stage fluorite and (or) carbonate veins in several of the scar areas (figs. 9, 10).

[1]Sericite is a petrographic or field term for fine-grained muscovite that typically has X-ray diffraction patterns characteristic of illite.

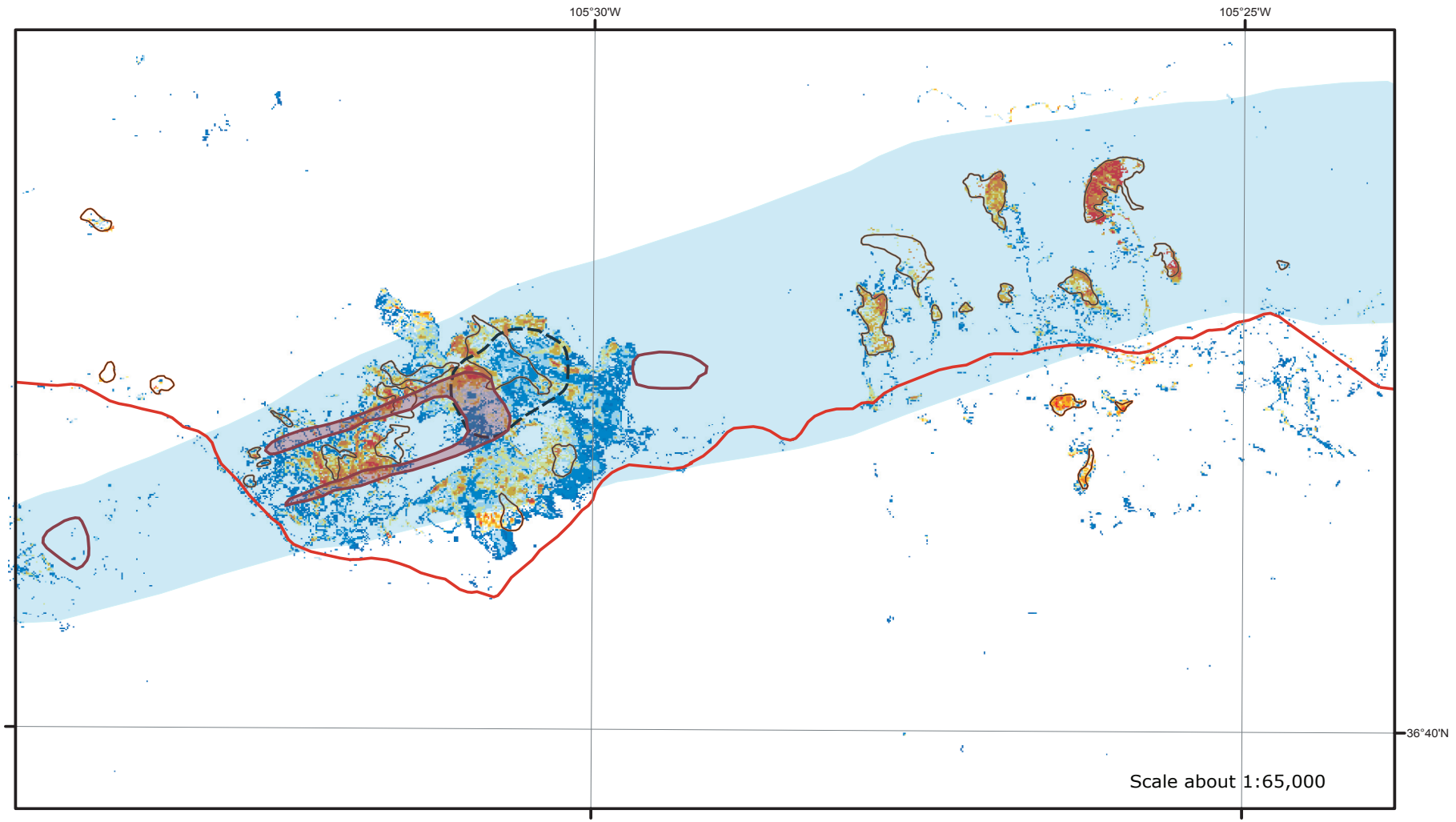

Figure 5. Map showing relative intensity of sericite alteration based on AVIRIS mapping. Bright orange, red, and yellow colors represent the strongest signal from sericite; dark blue and cyan indicate moderate sericite signal; and white indicates no signal from sericite. Bold lines are outlines of alteration scars from figure 2. Mined or known orebodies are outlined in maroon. Light blue overprint shows fluorine content greater than 1,000 ppm (from Robertson GeoConsultants, 2001). Red line is New Mexico Highway 38. Locations are approximate because AVIRIS data have not been adjusted to planimetric datum.

Propylitic alteration associated with the molybdenite ore deposits in part spatially overlaps and in part occurs peripherally to QSP alteration (fig. 6). Propylitically altered rocks contain chlorite, epidote, albite, and calcite and are typically greenish in color (fig. 7). The propylitic alteration is best developed in andesites and quartz latite porphyries (fig. 7) and is relatively poorly developed in the Amalia Tuff and rhyolite porphyries. These differences presumably resulted because the more silicic tuff and rhyolite porphyries had less Ca, Mg, and Fe to form abundant chlorite and epidote than the andesites and quartz latite porphyries.

At Questa, an older propylitic alteration—not linked to the molybdenite mineralization—regionally affected the volcanic rocks of the Latir field. This regional propylitic alteration especially affected the more mafic precaldera volcanics. It can be quite difficult to distinguish propylitic alteration that is distal to the magmatic hydrothermal molybdenum deposits from the regional propylitization.

QSP alteration associated with the molybdenite mineralization very commonly overprinted or partially replaced previous propylitic alteration of the andesites (figs. 7, 8). As a result, most mineralized and altered andesites peripheral to the main ore zones typically contain mixed QSP-propylitic alteration assemblages. Depending upon the extent of the QSP alteration, a mix of quartz, pyrite, and sericite is observed in hand samples and thin sections to replace feldspars, chlorite, carbonates, and epidote. Large areas of preserved propylitic-dominated alteration assemblages are therefore actually quite limited within the Red River mineralized trend. Areas high on the west wall of the open pit and within the downdropped Spring Gulch block east of the mine site near La Bobita campground (see fig. 4 cross section) are two of the rare areas where propylitic alteration has not been extensively overprinted by QSP alteration.

AVIRIS remote-sensing maps (Livo and Clark, 2002) have been instrumental in identifying localized occurrences of advanced argillic alteration in some of the alteration scars and over a broad area around the summit of Sawmill Mountain previously mapped by Loucks and others (1977). At least two types of advanced argillic alteration can be identified (fig. 7*C*, fig. 11), although their genetic and temporal relationships to the molybdenite mineralizing systems are unclear. Samples from several scar areas show that veins of alunite or kaolinite are common in the Amalia Tuff distal to the mineralizing intrusions; however, samples of drill core from beneath the Hottentot scar area indicate that the alunite and kaolinite veins diminish with depth, with a corresponding increase in intensity of QS and QSP alteration (fig. 7*C*). A distinctly different, previously unidentified, style of advanced argillic alteration was also located by the AVIRIS mapping in several relatively localized zones of brecciated rocks, including one on the Molycorp mine site and several near the Questa ranger station (fig. 11). Mineralogical studies of samples from these areas indicate that alunite, pyrophyllite, and kaolinite occur both in the matrix and clasts of the breccias. Both advanced argillic alteration types contain much less pyrite than the QSP-altered rocks. Further work is needed to understand the origin of (1) both styles of advanced argillic alteration and (2) the localized brecciation.

District-Wide Alteration Zoning

A district-wide map of surface alteration assemblages at Questa is not available. However, AVIRIS remote-sensing maps (Livo and Clark, 2002), when linked with results of field observations and mineralogical characterization studies, provide an idea of general alteration patterns across the district and the complexity of the patterns. For example, figure 5 includes AVIRIS results depicting the relative intensity of sericitic alteration exposed in unvegetated areas; it therefore provides an indication of the intensity of QSP alteration across the district. Similar AVIRIS maps of the Red River mineralized trend (not shown) indicate that calcite and epidote—indicative of propylitic alteration—are present within and surrounding areas of moderate to strong sericite signal intensity, consistent with the overprinting of QSP alteration assemblages onto propylitic assemblages commonly observed in thin sections. The AVIRIS data also show increased signals for propylitic-alteration minerals in the downdropped Spring Gulch block east of the mine site. As noted previously, the AVIRIS maps show extensive areas of kaolinite where the Amalia Tuff crops out along ridge crests and show a broad area over Sawmill Mountain with signals indicative of alunite and kaolinite.

District-Wide Geochemical Patterns at Questa

The only systematic geochemical data available for altered rocks in the Red River mineralized areas are portrayed in a series of maps presented in Robertson GeoConsultants (2001; their figs. 2.4–2.10). These maps, based on historic sampling of soils and rocks throughout the district, yield important insights about the geometry and continuity of the geochemical system at Questa.

The maps for Mo, F, Sn, and Pb are all similar and show anomalies for those elements in an elongate band that replicates the N. 75° E. trend of intrusions, mineral deposits, and hydrothermal alteration described earlier in this report (figs. 3, 4, and 5). Tin and fluorine are well-known "pathfinder" elements for Climax-type molybdenite deposits, and their elongate, linear distribution is unique here at Questa. Lead is not so commonly enriched in Climax-type hydrothermal systems, but the Robertson GeoConsultants (2001) lead map shows a number of anomalies > 100 ppm that mimic the pattern of Mo, Sn, and F.

The map depicting fluorine content of surface rocks presented in Robertson GeoConsultants (2001; their fig. 2.4) also provides important information about the true distribution of sericite and, as a result, QSP alteration. Based on the study by Gunow and others (1980) at the Henderson mine in Colorado, we can infer that the majority of fluorine released during emplacement of a Climax-type molybdenite deposit

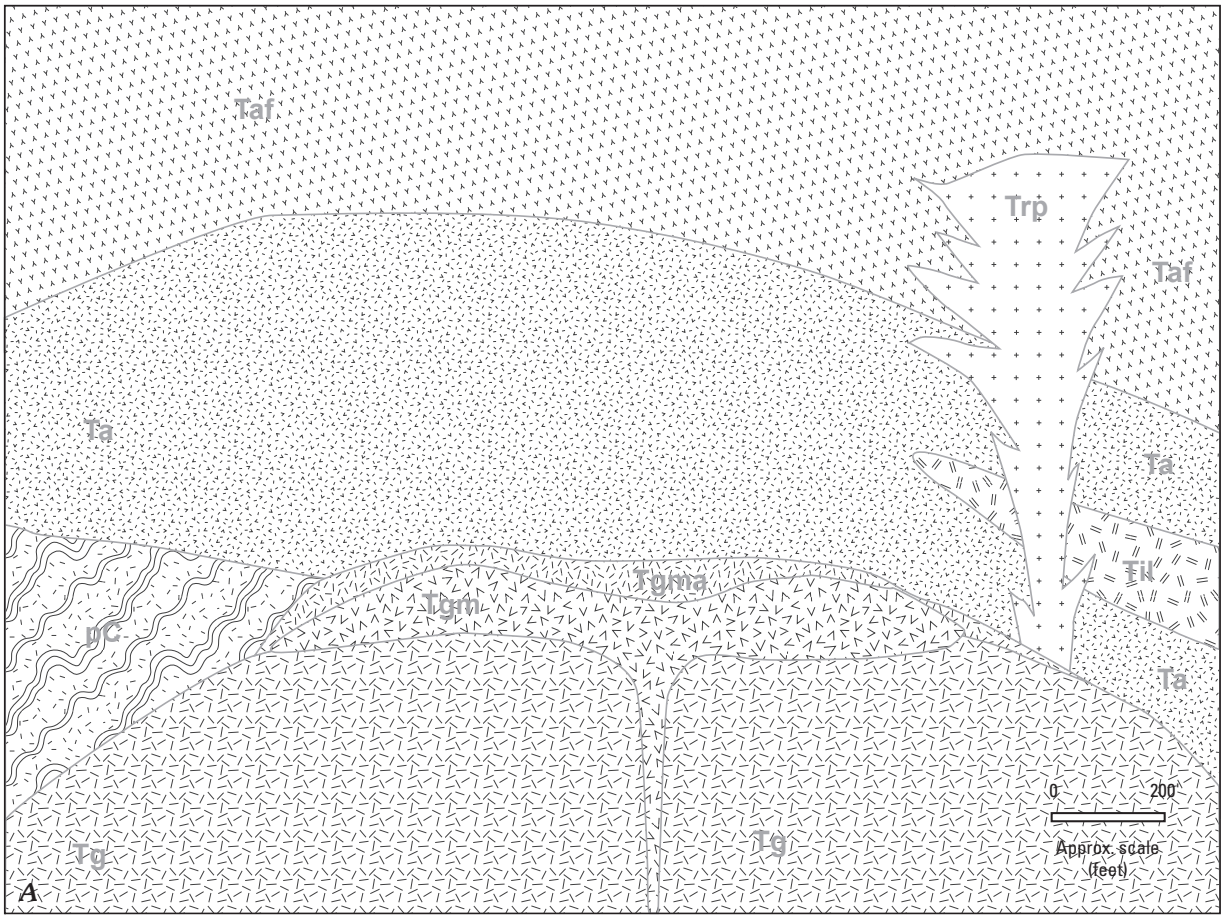

Figure 6. Cross sections showing *A*, inferred schematic spatial distributions of rock types; *B*, hydrothermal alteration types; and *C*, scar-area erosion levels around an idealized intrusion/mineralization center at Questa. These cross sections are modified from ones developed by Martineau and others (1977) based on geologic relationships they observed or inferred for the southwest orebody on the Questa mine site. Our cross sections integrate information on alteration assemblages and zoning patterns observed in this study in each of the various scar areas and in the Molycorp open pit. The scar-area erosion levels (*C*) are not to scale horizontally or vertically, nor are they meant to imply that all scar areas are developed around a single intrusive center; rather, they are meant to convey information about the types of alteration exposed in each of the scar areas.

Hydrothermal alteration
(listed in order of increasing proximity to source intrusion)

- Alunite and kaolinite of unknown age as veins and partial alteration of Amalia Tuff.
- Propylitic alteration, primarily of andesite and quartz latite porphyry rocks, to chlorite, sodium plagioclase, epidote, and calcite.
- Quartz-sericite (QS) alteration (orange): Distal, sulfide-poor facies of QSP alteration in rhyolitic intrusions and Amalia Tuff.
- Quartz-sericite-pyrite (QSP) alteration (brown): Generally incomplete alteration of rock to quartz, pyrite, and illite, with stockwork veins containing quartz, pyrite, and lesser chalcopyrite, pyrrhotite, carbonates, fluorite, barite, phosphates, Fe-Ti oxides. Intensity of alteration and veining diminishes away from source intrusions. Typically overprints propylitic alteration.
- Late-stage fluorite-carbonate veins.
- Magnetite-hematite-quartz stockwork veining
- Molybdenite (± quartz, pyrite, phlogopite) veins in rock potassically altered to contain phlogopite, potassium feldpsar, topaz, and other minerals

Rocks
(listed in order of increasing age)

- Source intrusion for mineralization (Tgm)
- Early aplites (Tgma)
- Early granites (Tg)
- Early rhyolite porphyry intrusions (Trp)
- Amalia Tuff (Taf)
- Quartz latite porphyry intrusions (Til)
- Andesites and associated volcaniclastic rocks (Ta)
- Precambrian (pC)

Mallette

Schematic erosion levels in different scar areas

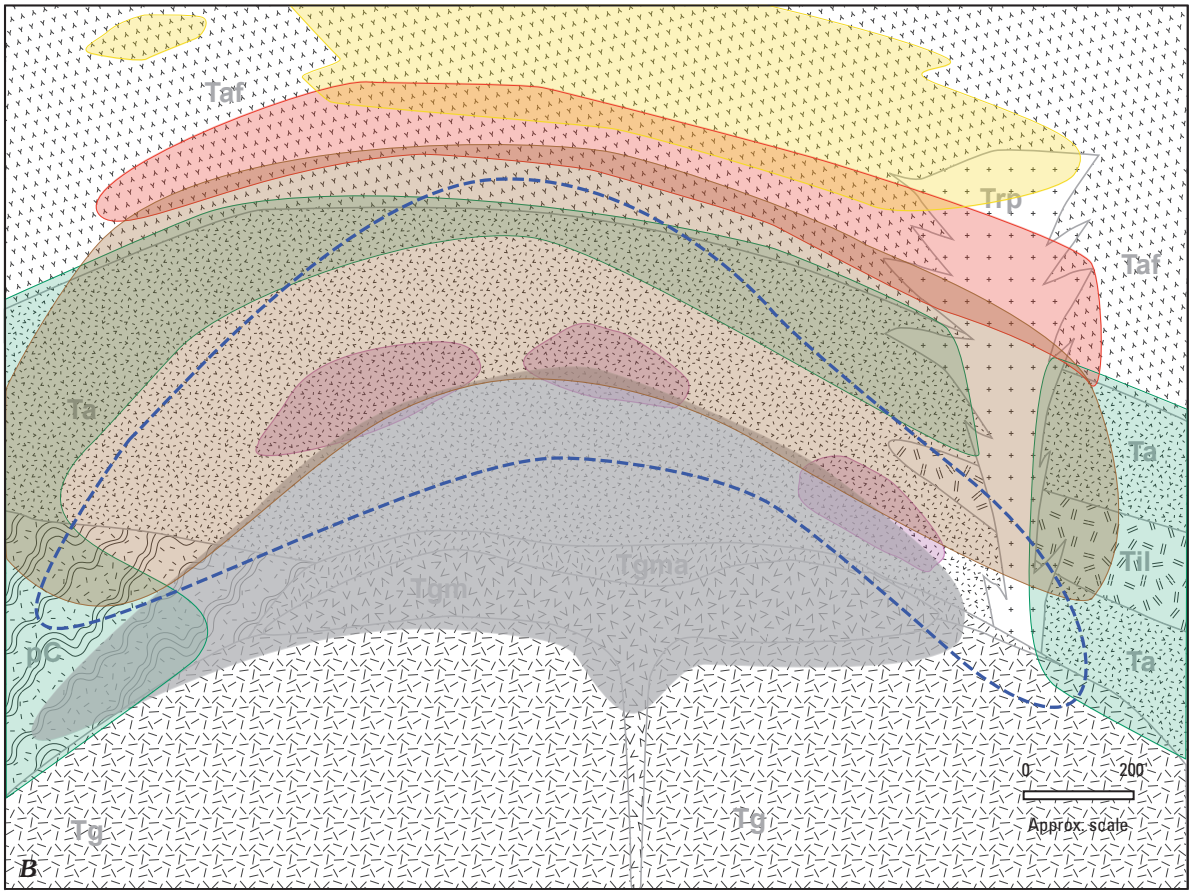
Taf
Trp
Taf
Ta
Ta
Tgma
Tgm
Tl
Ta
Tg
Tg
0
200
Approx. scale
B

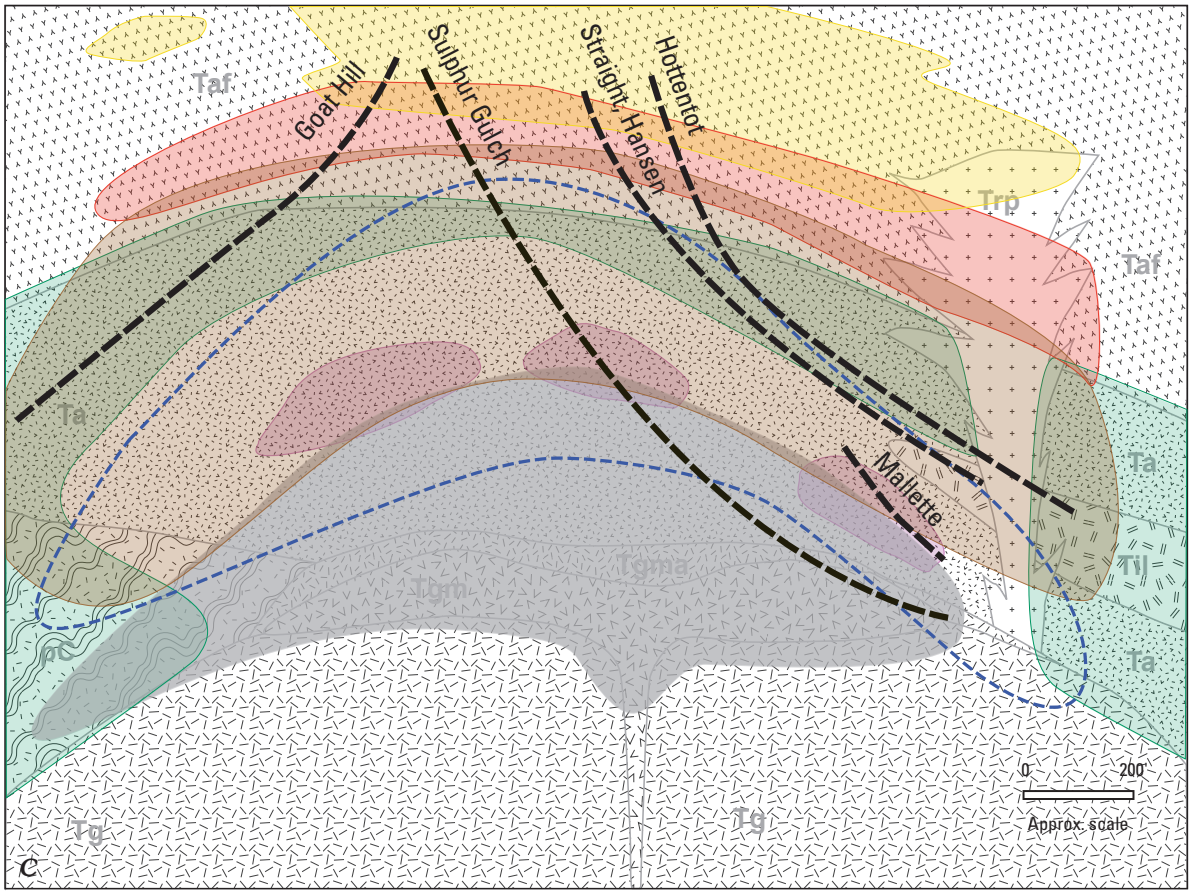
Goat Hill
Sulphur Gulch
Straight Hansen
Hottentot
Mallette
Taf
Trp
Taf
Ta
Ta
Tgma
Tgm
Tl
Ta
Tg
Tg
0
200
Approx. scale
C

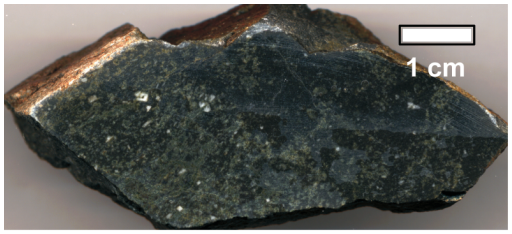

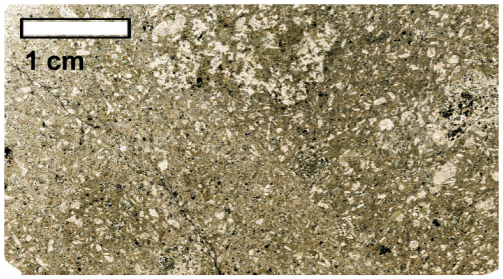

Sample Q10-18-02-6b. La Bobita picnic ground (HS-upper, TS-lower). Propylitic with no QSP. Plagioclase crystals (white in HS, and light tan in TS) are partly replaced by greenish epidote. Green chlorite replaces pyroxenes. Small black minerals in TS are iron- and iron-titanium oxides from the original andesite. Pyrite is absent.

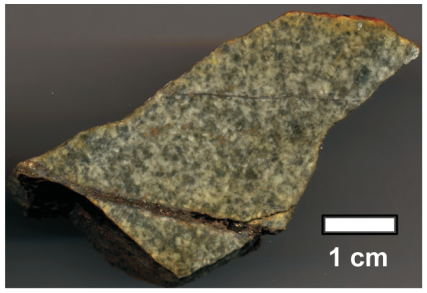

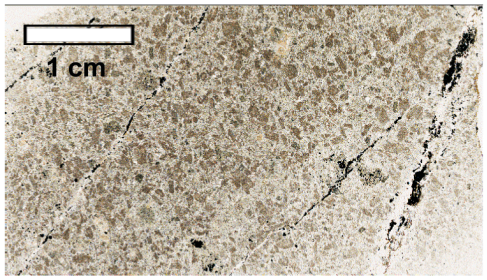

Sample Q10-17-02-1c, Straight Creek (HS-upper, TS-lower). Propylitic overprinted by QSP and late carbonate. Tan plagioclase crystals in HS are seen in TS to be partly replaced by brown sericite/illite. Chlorite remaining in the sample imparts a greenish tint in HS and TS. Black minerals in TS are nearly all pyrite. Several quartz-pyrite veins are visible in TS.

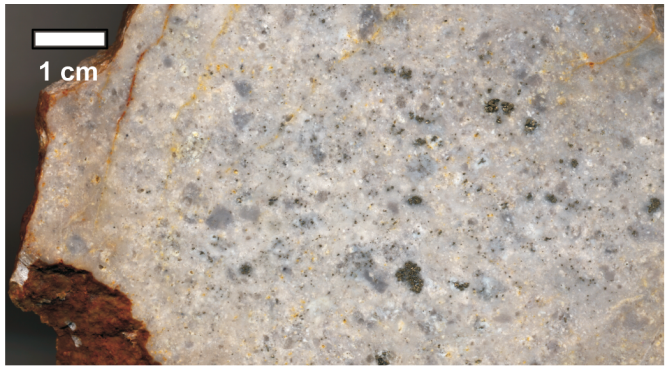

Sample Q10-18-02-4a, SE Straight Creek. Relatively intense QSP alteration. Dark clots are pyrite, white specks are plagioclase mostly replaced by fine sericite/illite.

Sample Q10-01-1, Upper Straight Creek. Relatively intense QSP, crosscut by stockwork quartz (gray) and pyrite (greenish gold) fractures.

Figure 7*A*. Hand sample (HS) and transmitted-light photographs of thin sections (TS) showing progressive alteration of andesite from propylitic (left) through more intense quartz-sericite-pyrite (QSP, right).

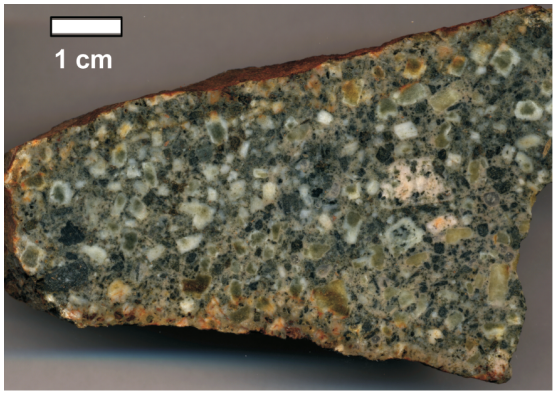

Sample Q10-15-02-2, June Bug. Propylitic with little QSP. Plagioclase crystals (light gray) are partly replaced by greenish epidote. Green chlorite replaces pyroxenes. Pink crystals are potassium feldpar.

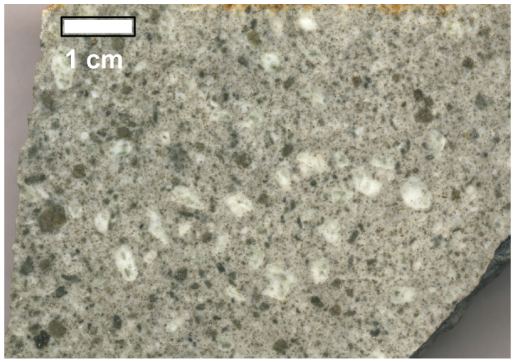

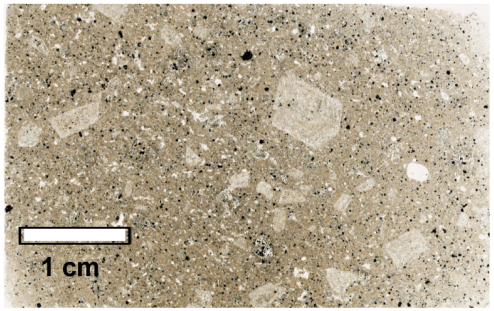

Sample Q10-15-02-1A, June Bug (HS-upper, TS-lower). Propylitic overprinted by QSP alteration. Plagioclase crystals (light gray in HS, tan in TS) are partly replaced by illite/sericite (brown in TS). Green chlorite is still present where it replaced pyroxenes. White crystals in TS are original quartz crystals from the porphyry. Black minerals in TS are pyrite.

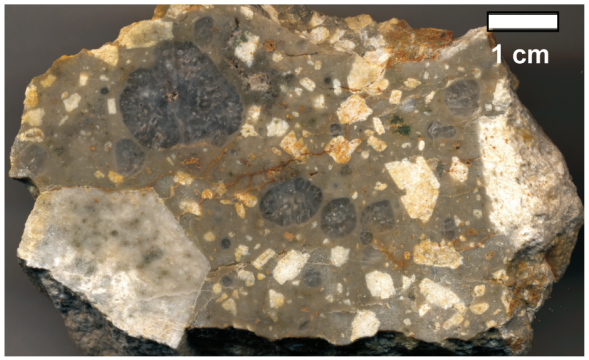

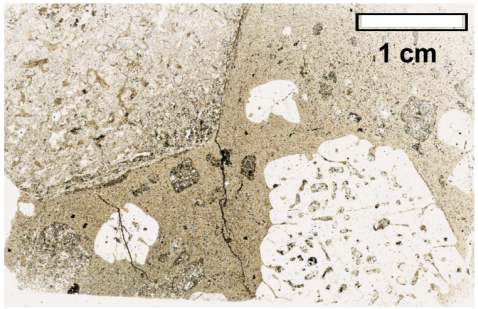

Sample Q10-16-02-1, Hottentot (HS-upper, TS-lower). Abundant QSP with remnant propylitic alteration of a coarse phase of the porphyry. Large euhedral feldspar crystals and the groundmass are largely replaced by illite/sericite (white in HS, brown in TS). Rounded resorbed quartz crystals (gray in HS, white in TS) remain from the original rock. Fine-grained chlorite is still present in the rock. Black mineral in TS is pyrite.

Propylitic → Mixed propylitic and QSP → QSP > Propylitic

Figure 7*B*. Hand sample (HS) and transmitted-light photographs of thin sections (TS) showing progressive alteration of quartz latite porphyry from propylitic (left) through more intense quartz-sericite-pyrite (QSP, right).

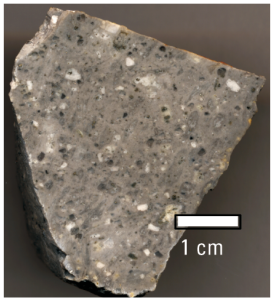

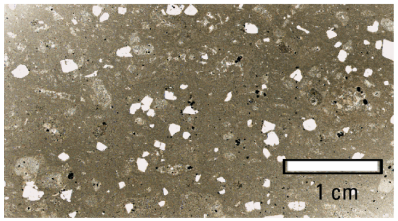

Sample Q02-20, Upper Goat Hill, the Narrows (HS-upper, TS-lower). More intense alteration of Amalia to QSP, primarily manifested as silicification and pyritization. Much of the original foliation and pumice fragments have been destroyed. Disseminated pyrite comprises ~4% of rock.

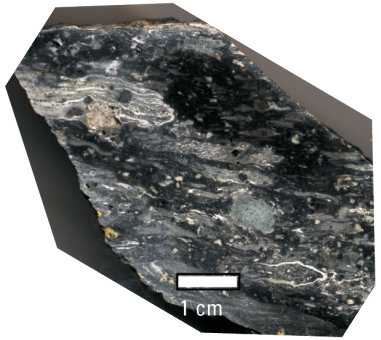

Sample Q02-4, Sulphur Gulch, upper W open pit. Partly altered to QSP. Illite/sericite (white) is preferentially altering the pumice fragments (gray). Disseminated pyrite comprises ~1% of rock.

Sample Q10-17-02-9, West Goat Hill. Partial alteration of Amalia to QSP. Disseminated pyrite comprises ~1% of rock.

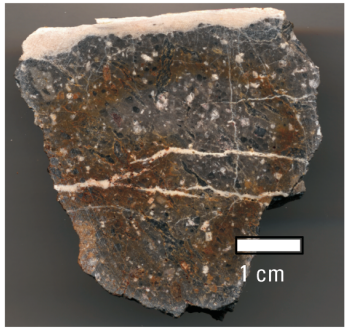

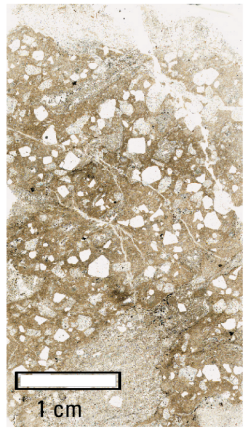

Sample Q10-16-02-3, Hottentot (HS-upper, TS-lower). Pink veins of alunite cut Amalia Tuff. Some partial alteration of groundmass and pumice fragments to alunite has also occurred. Opaques in TS are iron- and iron-titanium oxides. Pyrite is absent.

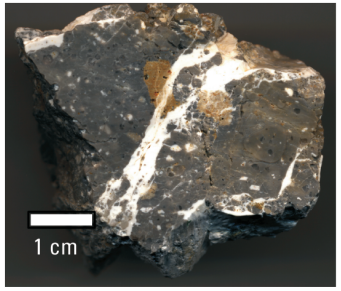

Sample Q6-01-2, Uppermost Hottentot. White veins of kaolinite cut Amalia Tuff. Minor alteration of groundmass and pumice fragments to kaolinite may also have occurred. Pyrite is absent

More intense QSP

Less intense QSP

Advanced argillic / argillic

Increasing elevation or distance from the mineralizing granitic intrusions? ⟹

Figure 7*C*. Hand sample (HS) and transmitted-light photographs of thin sections (TS) showing possible spatial variations in alteration of Amalia Tuff, possibly with increasing distance or elevation (shown from left to right on figure) from granitic intrusions that were sources for molybdenum mineralization. However, it is not clear whether argillic and advanced argillic alteration is related genetically or temporally to molybdenum mineralization.

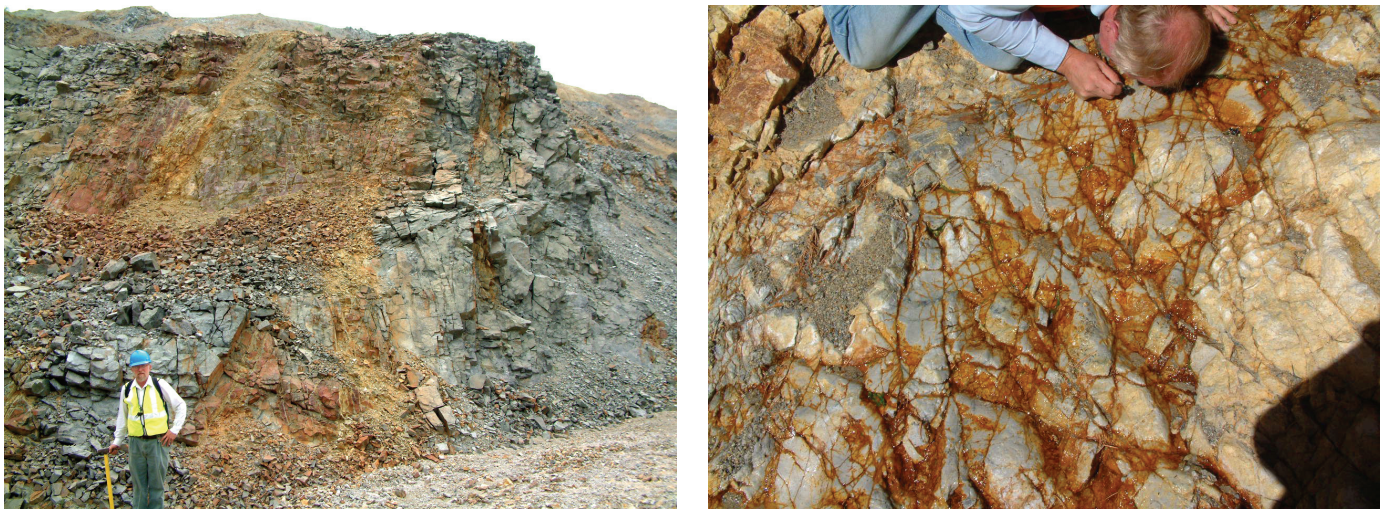

A *B*

Figure 8. *A*, view of mine bench on the upper west wall of Molycorp open pit showing zone of QSP alteration crosscutting earlier propylitically altered andesite. QSP alteration is manifested on the surface by orange iron oxides and hydroxides generated by oxidation of pyrite. *B*, stockwork fractures in QSP-altered andesite, Straight Creek scar. Bright orange colors highlight acid waters flowing along fractures in stream channel. The volume of water gradually increased downstream from this locality, suggesting possible inflow of ground waters into the stream from shallow subsurface.

will be fixed in hydrothermal muscovite (sericite) in the QSP zone, in fluorite in veinlets cutting the QSP zone, and in the potassic zone (where much of the fluorine is found in biotite). We infer that most of the fluorine depicted on the Robertson GeoConsultants map outside of the main mine site is present in mineralization-related sericite and fluorite, and we have generalized their map to produce the overlay (F > 1,000 ppm) portrayed in figure 5. This fluorine distribution corresponds closely to known mineral deposits, stocks, and alteration scars and provides another indication that the QSP alteration is fairly continuous along the length of the N. 75° E. trend.

The Robertson GeoConsultants (2001) geochemical maps for Cu, Zn, and Mn show distinctly different patterns than those for Mo, Sn, and F; anomalous Cu, Zn, Pb, and Mn values are present only above the Central (Goat Hill) orebody, on the margin of the existing open pit, and to the west on Goat Hill. These three elements, like Pb, are not diagnostic of Climax-type systems, and their presence here, along with Pb, serves to underline the variability within mineral-deposit types and suggests that Questa, for whatever reason, may be richer in base metals than most Climax-type systems.

Geology and Alteration of Red River Alteration Scars

The Red River alteration scars form as a result of rapid chemical weathering and physical erosion of pyrite-rich hydrothermally altered rocks along the N. 75° E. trend above the inferred batholith (figs. 4, 5). As noted by Meyer and Leonardson (1990), so-called "divide" scars form at higher elevations along the main E.-W. ridge crests on both sides of the Red River. "Inner valley" scars generally form at lower elevations along the break in slope between the inner Red River canyon and the broader outer valley, primarily on the noses of ridges between the divide-scar drainages.

There is some disagreement in the literature on the names given to the alteration scars. Most of the scars were named by Meyer and Leonardson (1990), with sometimes different names provided by Robertson GeoConsultants (2001). We have generally followed the Meyer and Leonardson (1990) nomenclature. In addition, we have named some previously unnamed scars, applying some of the same conventions used by Meyer and Leonardson (1990).

From west to east, the major divide alteration scars include (fig. 2) Hansen, Straight, South June Bug, and Hottentot. The major inner valley alteration scars, from west to east, include Questa, Eagle Rock, South Goat Hill, Goat Hill, South Truck Shop (also known as Sugar Shack), Southeast Truck Shop (also known as Old Sulphur), Sulphur Gulch, Southwest Hansen, South Straight, Southeast Straight, June Bug, East June Bug, and Southeast Hottentot. Alteration scars east of the village of Red River include Mallette, Lower Bitter Creek, and Bitter Creek. Mechanisms by which the alteration scars form will be presented in a subsequent section. Here, we compare the salient geologic and geochemical characteristics of the alteration scars. An overall summary of key characteristics of each of the alteration scars is presented in table 1.

Each of the Red River alteration scars is distinctive in terms of its topography, size, and the proportion and distribution of various rock types and hydrothermal mineralization

Q02-19, Open pit below Sulphur Gulch. Green fluorite coated by later pink manganiferous carbonate from a vein cutting granite.

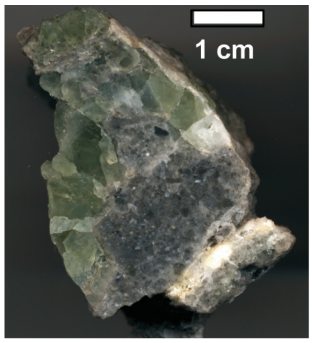

Unnumbered sample, from float in Straight Creek scar. Green and tan fluorite coat QSP-altered andesite.

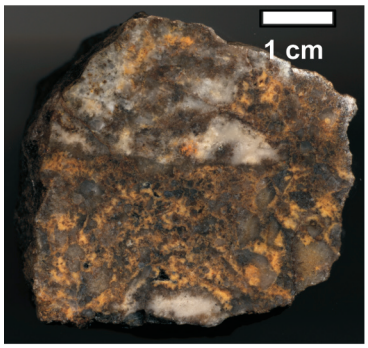

Q10-18-02-4b, SE. Straight. Carbonate-quartz vein cutting QSP-altered andesite.

Q10-15-02-1, June Bug. Abundant late calcite cementing breccia fragments of propylitically altered quartz latite porphyry.

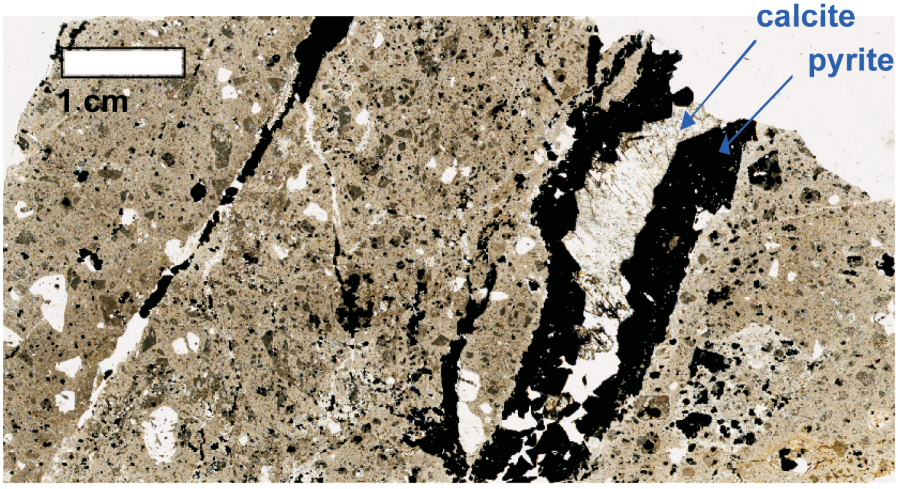

Figure 9. Hand sample photographs (upper and middle) and thin section photomicrograph (bottom) of late-stage carbonate and (or) fluorite veining from the Molycorp open pit and various scar areas.

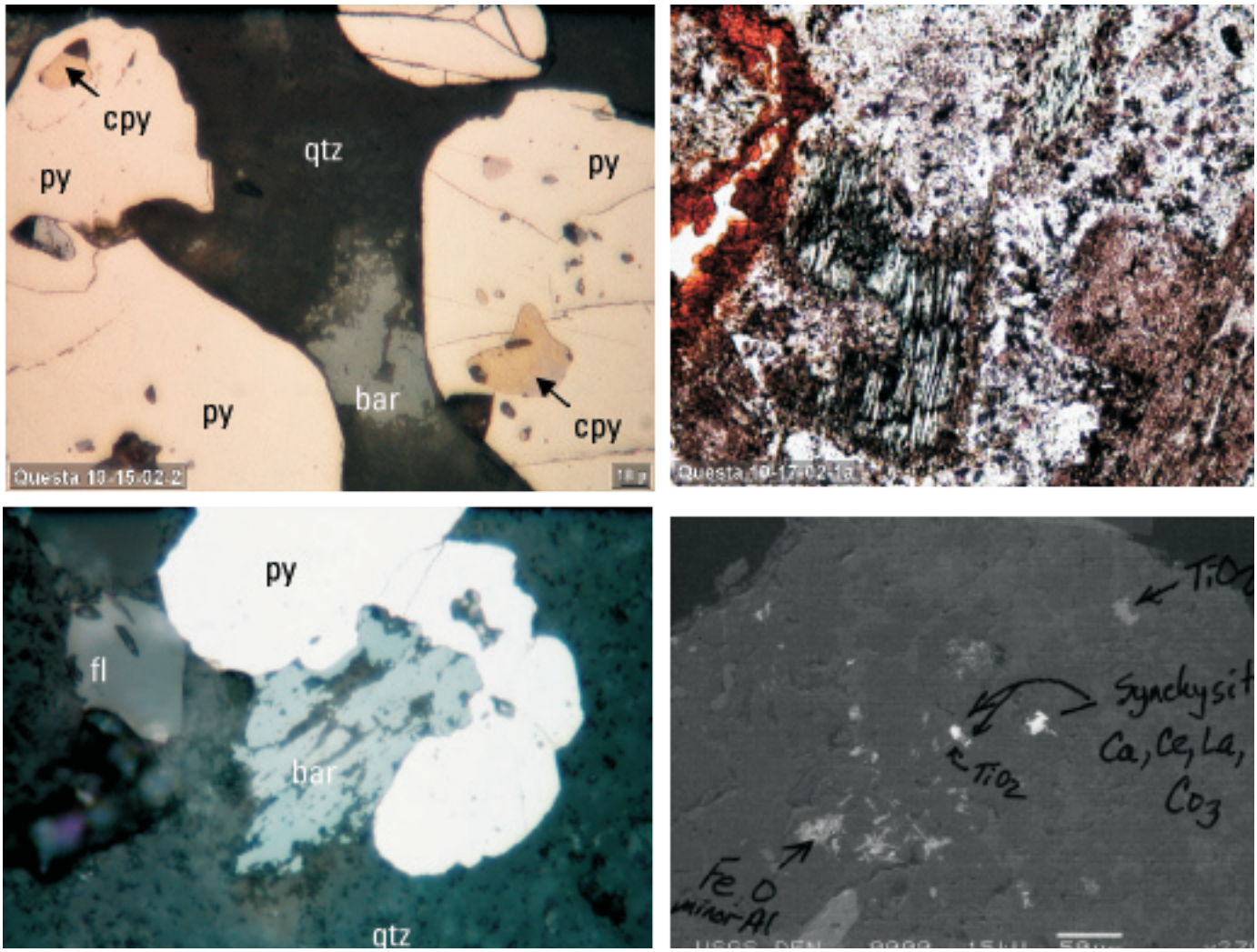

Figure 10. Upper left—Q10-15-02-2, June Bug. Reflected-light photomicrograph showing hydrothermal pyrite (py), chalcopyrite (cpy), barite (bar), and quartz (qtz) from a vein in QSP-altered and propylitically altered quartz latite porphyry. Lower left—Q02-20, Goat Hill. Reflected-light photomicrograph showing hydrothermal pyrite (py), barite (bar), fluorite (fl), and quartz (qtz) from a vein in QSP-altered Amalia Tuff. Upper right—Q10-17-02-1a, Straight Creek. Transmitted-light photomicrograph of QSP-altered and propylitically altered andesite showing chlorite (green) replaced on its rims by later illite (bronze), plagioclase laths replaced by illite (bronze, blocky), groundmass quartz (white), and a secondary vein of goethite (orange). Lower right—SC5B-277, Straight Creek drill hole. SEM backscattered electron photomicrograph of QSP-altered and propylitically altered quartz latite showing late hydrothermal rare-earth carbonate, Fe oxides, and Fe-Ti oxides.

and alteration types. Nonetheless, some commonalities exist between all of the alteration scars, particularly in the occurrence of common rock and alteration types (table 1).

Bedrock Geology

Andesite volcanic and volcaniclastic rocks crop out in most of the alteration scars and are the dominant rock types in the South Goat Hill, Sulphur Gulch, SW. Hansen, Straight, and South and Southeast Straight scars. Amalia Tuff is the dominant bedrock unit mapped in the Questa, Hansen, and Goat Hill scars. Quartz latite porphyry is the dominant rock type in the June Bug and SE. Hottentot scars; it is also present within the Straight scar and at depth below the Straight Creek debris fan (encountered in the SC-1 through SC-5 drill holes). In nearly all of the alteration scars, granitic rocks associated with mineralization do not crop out at the surface but have been encountered locally in drill holes in the subsurface; the primary exception is the Sulphur Gulch scar, in which granitic rocks and associated high-grade molybdenum mineralization were exposed by erosion in the lower portions of the alteration scar prior to mining.

In most of the divide alteration scars, ridge crests are capped by Amalia Tuff. Andesites and, to a lesser spatial extent, quartz latite porphyries and rhyolite porphyries form the slopes on most of the divide and inner valley scars. Visual observations of the Hansen scar suggest that, although the

Table 1. Key characteristics of Red River scar areas, most sampled as part of this study.

[Geologic information on the Questa, S. Truck Shop, and SE. Truck Shop scar areas is from the literature. Geochemically anomalous elements from Robertson Geoconsultants, Inc. Abbreviations: py, pyrite; cpy, chalcopyrite; po, pyrrhotite; mol, molybdenite; adv. QSP, advanced quartz-sericite-pyrite alteration; prop, propylitic alteration; adv. arg, advanced argillic alteration; arg, argillic alteration; rhyo. porph, rhyolite porphyry]

	Questa	West Goat Hill	Goat Hill	South Goat Hill	S. Truck Shop	SE. Truck Shop	Sulphur Gulch (pit)
Map area (m^2)	47,725	34,000	214,100	153,200	74,100	80,921	387,950
Max. elevation	8,850	8,700	9,830	9,400			10,200
Min. elevation	8,100	7,700	8,750	8,250			8,680
Facing	W.	SW.	SW.	S.	S.	SSE.	SSE.
Dominant rock type(s), from Lipman and Reed (1989)	Amalia	Amalia, rhyolite porphyry	Amalia	Amalia, andesite, rhyolite porphyry	Andesite, rhyolite porphyry, Precambrian metamorphics	Andesite, rhyolite porphyry, Precambrian metamorphics	Upper: andesite; Amalia. Lower: granite, rhyolite porph.
Alteration type(s)	QSP?	QSP	QSP	QSP overprinting prop	Infer QSP overprinting prop	Infer QSP overprinting prop	Upper: QSP overprinting prop Lower: potassic
Sulfides near surface	Not sampled	Py; Minor cpy?	Py	Py	Not sampled	Not sampled	Upper: py; cpy Lower: mol
Carbonates in rock near surface?	Not sampled	None yet detected	Y (trace)	Not evaluated	Not sampled	Not sampled	Y
Geochemically anomalous elements		Sn (±Mn, F, Mo)	F, Pb, Zn, Cu, Mn, Mo, Sn	F, Pb, Zn, Cu, Mn, Mo, Sn	No data?	No data?	Upper: No data? Lower: F, Mo, Mn?

Table 1. Key characteristics of Red River scar areas, most sampled as part of this study—*Continued*.

	SW. Hansen	Hansen	Straight	June Bug	SE. Straight	Hottentot	SE. Hottentot
Map area (m^2)	194,150	233,450	168,663	56,000	90,850	253,200	56,550
Max. elevation	9,750	10,550	10,100	9,400	9,500	10,791	9,900
Min. elevation	8,700	8,950	9,200	8,800	8,950	9,800	9,150
Facing	S.	S.	S.	N.	S.	S.	SW.
Dominant rock type(s), from Lipman and Reed (1989)	Andesite, minor rhyolite porphyry, minor Amalia	Amalia; andesite	Andesite; rhyolite porphyry; Amalia	Qtz. latite porph.	Andesite	Rhyolite porphyry, Amalia	Qtz. latite porph.
Alteration type(s)	QSP overprinting prop	Andesites: QSP overprinting prop Amalia: some adv. arg?	Andesite: QSP overprinting prop Amalia: adv. arg	QSP overprinting prop; possibly some arg	QSP overprinting prop	Rhyo. porph: QSP overprinting prop Amalia: arg, adv. arg	QSP overprinting prop; adv. arg
Sulfides near surface	Py	Py	Py, minor po, cpy	Py, minor po, cpy	Py, minor po, cpy.	Py	Py
Carbonates in rock near surface?	Y	None yet detected	Y	Y	Y	Not evaluated	Not evaluated
Geochemically anomalous elements	Minor F, Mo	Minor F, Mo	F, Pb, Mo, minor Sn		F, Mo, Pb	F, Mo, minor Sn and Pb	F, Pb

Table 2. X-ray diffraction results on selected hand samples or drill cutting samples showing how major mineralogy varies as a function of rock type, alteration type, and scar area.

[Samples were prepared by adding 10 percent (mass basis) ZnO, which was used to normalize X-ray diffraction (XRD) patterns. A selected suite of standard minerals was then fit to the sample pattern by least squared-difference using RockJock, a macro-driven program written for Excel (Eberl, 2003). *, mineral identified quantitatively by XRD but present below significant quantitative percentage (<0.5 percent). Mineral totals substantially greater than 100 percent may result from background effects of X-ray-generated pyrite fluorescence. Leaders (--) indicate mineral not included in calculated model]

	Goat Hill		Sulphur Gulch/open pit				SW. Hansen	
Sample	**Q02-20**	**Q02-21**	**Q02-7**	**Q02-8**	**Q02-15-0**	**Q02-15-U0**	**9125 gray**	**9125 buff**
Rock type	Amalia	Amalia	Andesite	Andesite	Peralk. rhyo flow	Peralk. rhyo flow	Qtz. latite?	Andesite
Alteration type(s)	QSP	QSP	Prop > QSP	Prop > QSP	QSP, prop	QSP, prop	Prop, QSP	QSP > prop
Mineral	Weight %	Weight %	Weight %	Weight %	Weight %	Weight %	Weight %	Weight %
Quartz	49.2	56.4	24.9	22.8	36.1	30.2	24.1	50.2
Microcline feldspar	6.9	9.4	8.0	3.8	4.2	3.7	4.7	2.4
Sanidine feldspar	13.7	11.4	13.4	15.1	7.9	5.1	9.8	--
Albite feldspar	10.4	--	20.8	22.4	10.6	8.1	17.5	16.9
Oligoclase feldspar	1.1	--	13.8	14.4	11.6	21.2	15.2	2.9
Andesine feldspar	2.0	--	--	--	--	3.7	--	--
Plagioclase total	13.5	--	34.6	36.8	22.2	33.0	32.7	19.8
Rutile	0.7	--	*	*	0.4	0.7	--	0.1
Magnetite	--	*	--	--	--	--	--	0.1
Calcite	--	--	*	--	--	--	1.0	--
Pyrite	3.4	--	1.1	1.1	1.4	3.1	2.6	1.8
Anhydrite	0.7	0.8	*	--	*	*	*	0.3
1M illite	9.4	11.5	5.5	6.6	12.9	13.3	9.6	10.3
2M1 illite	2.5	8.1	--	--	2.4	--	1.8	9.8
Biotite (1M)	--	2.1	0.6	--	1.4	1.4	--	1.6
Phlogopite (2M1)	4.6	2.7	3.6	2.4	4.3	2.0	1.7	4.6
Chlorite total	3.0	2.5	9.3	8.1	8.9	7.0	4.1	4.5
Fluorite	*	--	*	*	*	*	*	--
Epidote	0.7	*	2.1	2.4	1.5	*	1.3	0.1
Hematite	*	--	*	*	*	*	--	--
Disordered kaolinite	3.2	1.2	--	0.5	3.3	--	--	6.7
Ferruginous smectite	1.5	--	--	*	--	1.3	--	2.6
Jarosite	--	--	--	*	1.2	--	--	--
Goethite	--	--	--	--	--	--	--	--
Gypsum + bassanite	*	0.6	1.7	2.1	0.8	1.1	1.5	*
TOTAL	**113.6**	**107.2**	**105.7**	**102.7**	**109.7**	**102.8**	**95.4**	**115.1**

Table 2. X-ray diffraction results on selected hand samples or drill cutting samples showing how major mineralogy varies as a function of rock type, alteration type, and scar area—*Continued*.

Sample	Q10-17-02-1a	Q10-17-02-1b	Straight Moss	Straight Upper Straight	10-17-02-3	10-17-02-4	10-17-02-6	10-17-02-7
Rock type	Andesite	Andesite	Qtz. latite?	Andesite	Andesite	Qtz. latite?	Andesite	Andesite?
Alteration type(s)	QSP > prop	QSP > prop	Prop, QSP	QSP >> prop	QSP > prop	Prop, QSP	QSP > prop	Qsp, prop
Mineral	Weight %	Weight %	Weight %	Weight %	Weight %	Weight %	Weight %	Weight %
Quartz	36.1	39.4	23.3	44.5	56.6	25.9	34.8	28.3
Microcline feldspar	--	--	6.5	6.0	--	4.8	4.0	6.4
Sanidine feldspar	--	--	13.0	0.9	*	13.9	0.4	18.1
Albite feldspar	--	--	21.5	14.9	--	16.8	5.2	26.9
Oligoclase feldspar	--	--	14.5	--	--	8.7	1.9	11.8
Andesine feldspar	--	--	--	--	--	--	0.1	1.2
Plagioclase total	14.5	6.8	36.0	14.9	0.6	25.5	7.2	39.9
Rutile	0.5	--	*	*	*	--	--	0.4
Magnetite	--	--	--	--	--	--	--	--
Calcite	*	2.9	1.1	0.6	0.7	0.9	--	--
Pyrite	2.8	4.8	4.7	5.1	2.7	1.7	2.3	3.4
Anhydrite	--	--	*	*	0.6	0.4	--	0.6
1M illite	9.7	5.1	7.2	16.5	25.0	7.6	25.1	14.5
2M1 illite	15.2	25.2	1.2	6.8	5.3	--	3.4	--
Biotite (1M)	--	--	--	--	--	0.5	0.3	0.7
Phlogopite (2M1)	--	--	--	3.3	2.0	1.9	5.0	4.4
Chlorite total	23.4	13.3	5.6	3.4	5.7	10.1	13.0	4.9
Fluorite	--	--	*	*	--	0.3	0.2	0.5
Epidote	--	--	1.3	--	--	6.6	--	--
Hematite	--	--	*	*	*	0.1	0.3	*
Disordered kaolinite	--	--	0.4	--	--	1.8	--	--
Ferruginous smectite	--	--	0.6	2.7	1.9	--	1.2	*
Jarosite	--	--	--	--	--	--	0.2	--
Goethite	0.5	0.5	--	--	--	--	--	*
Gypsum + bassanite	--	1.8	1.4	0.9	*	1.2	0.2	0.3
TOTAL	**102.9**	**99.2**	**103.6**	**106.6**	**101.6**	**103.3**	**97.6**	**110.5**

Table 2. X-ray diffraction results on selected hand samples or drill cutting samples showing how major mineralogy varies as a function of rock type, alteration type, and scar area—*Continued*.

Sample	Straight (continued) SC3B 180-185	Straight (continued) SC5B 320	Straight (continued) SC5B 390	SE. Straight 10-18-02-4B	June Bug 10-15-02-1A3	Hottentot 10-16-02-1	Hottentot 10-16-02-4	Hottentot 10-16-02-5
Rock type	Andesite	Qtz. latite porph?	Andesite?	Andesite	Qtz. latite porph	Qtz. latite porph	Amalia?	Qtz. latite porph
Alteration type(s)	QSP > Prop	Prop > QSP	Prop > QSP	QSP > Prop	QSP > Prop	QSP >> Prop	QSP	QSP
Mineral	Weight %	Weight %	Weight %	Weight %	Weight %	Weight %	Weight %	Weight%
Quartz	63.5	27.6	38.4	58.7	43.8	43.9	70.1	54.9
Microcline	0.4	5.4	3.5	1.2	0.5	0.8	--	0.7
Sanidine feldspar	1.1	13.0	1.7	6.1	1.0	3.2	--	0.7
Albite feldspar	--	22.3	22.4	--	1.5	--	--	--
Oligoclase feldspar	1.1	6.3	10.1	--	--	--	--	--
Andesine feldspar	0.9	*	--	--	0.5	--	--	--
Plagioclase total	2.0	28.7	32.5	--	2.0	--	--	--
Rutile	--	--	*	--	0.5	--	--	*
Magnetite	--	--	--	--	--	*	--	--
Calcite	--	1.2	--	--	--	--	--	--
Pyrite	0.9	1.5	1.8	2.8	3.0	*	1.1	3.8
Anhydrite	0.8	*	*	0.9	--	0.4	1.5	--
1M illite	12.1	1.3	7.5	16.8	19.6	19.5	--	22.2
2M1 illite	11.2	2.7	4.3	4.9	8.8	31.7	27.3	5.3
Biotite (1M)	1.2	--	--	2.0	*	--	8.4	1.8
Phlogopite (2M1)	1.5	0.5	2.4	2.5	3.7	--	--	1.3
Chlorite total	2.3	7.7	6.7	5.0	3.9	6.9	4.0	2.9
Fluorite	--	*	*	--	*	--	--	--
Epidote	--	6.1	0.3	*	0.9	--	--	*
Hematite	*	*	*	--	--	--	*	--
Disordered kaolinite	1.7	4.4	1.1	--	1.3	--	2.9	5.9
Ferruginous smectite	1.2	--	--	1.7	3.6	--	--	0.7
Jarosite	--	--	--	--	0.5	--	--	--
Goethite	--	--	--	--	--	--	--	--
Gypsum + bassanite	0.5	0.8	*	*	1.3	--	*	*
TOTAL	**100.6**	**101.5**	**100.7**	**103.2**	**94.7**	**106.7**	**104.3**	**100.9**

scar slopes are mapped as Amalia Tuff, the slopes are actually dominated by a series of slump blocks of Amalia Tuff overlying highly weathered andesite.

Relatively little is known about the nature of bedrock below the Red River; it is covered by river alluvium and debris flows issuing from the alteration scars. Recent drilling in the lower Straight Creek, Hottentot Creek, and Hansen Creek debris fans, carried out as part of the current USGS project, has reached bedrock and will provide some information on the subsurface bedrock in these areas.

Spatial Variations in Hypogene Mineralization and Alteration Between Scar Areas

Field observations and mineralogical characterization of samples collected from unoxidized bedrock exposures (table 2), coupled with AVIRIS mineral mapping (fig. 5) (Livo and Clark, 2002) provide further insights into the types and spatial distribution of hypogene mineralization and alteration developed in the Red River alteration scars.

It is apparent that nearly all of the andesite and quartz latite porphyry rocks within and surrounding the various alteration scars were propylitically altered, either regionally prior to mineralization or contemporaneously with, but distally to, mineralization (fig. 6). In contrast, samples of rhyolite porphyry and Amalia Tuff analyzed to date typically contain little chlorite (table 2) and seem to have not been particularly affected by the propylitization, perhaps because (1) of their low original iron and magnesium contents or (2) if most propylitic alteration actually predates the Amalia Tuff. AVIRIS (Livo and Clark, 2002) maps of carbonate and epidote signals indicate that the most intense areas of propylitic alteration along the lower Red River occur in the downdropped Spring Gulch block east of the mine site, on the ridge southwest of the open pit, and west of the Eagle Rock scar.

QSP alteration is a dominant alteration type in most of the Questa alteration scars (fig. 5). Alteration typically resulted in the addition of substantial silica (the most QSP-altered andesites have quartz contents around 60 weight percent) and pyrite (typically several weight percent, depending upon the abundance of pyrite-rich stockwork veins). In addition, silicate minerals were partially altered to fine-grained sericite (identified in XRD analysis as illite), with illite contents from 20 to 25 percent. However, as noted previously, QSP alteration only partially overprinted earlier propylitic alteration in the andesites and quartz latites. As a result, most andesites and quartz latites examined in this study were substantially less altered to QSP and have 20–35 percent quartz, less than 10 percent illite, and pyrite contents around several percent; higher proportions of the propylitic alteration assemblages remain in these samples, with as much as 30 percent plagioclase feldspar and 10–15 percent chlorite (table 2).

In the Upper Goat Hill, South Goat Hill, Sulphur Gulch, and SW. Hansen scars, the Amalia Tuff, where present closest to the mineralizing intrusives, is altered to QSP. The QSP alteration then grades distally upward and outward into QS alteration. Isolated occurrences of still more distal kaolinitic and alunitic advanced argillic alteration may be present at the highest elevations in the Goat Hill and Sulphur Gulch scars. To the east, AVIRIS mapping indicates that Amalia Tuff outcropping in the Hansen, Straight, Hottentot, and SW. Hottentot scars, and on top of Sawmill Mountain, contains advanced argillic alteration. Field and hand-sample observations show these outcrops are marked by veins of alunite, pyrophyllite, and (or) kaolinite (figs. 6, 7*C*) cutting Amalia Tuff, with lesser alteration of the groundmass to these minerals. Examination of drill core from the Hottentot area suggests that these advanced argillic assemblages grade vertically downward into QS and then QSP alteration of the Amalia Tuff.

Carbonates are common in all of the scar areas where QSP and (or) propylitic alteration is present. Although some of the carbonates are likely associated genetically with the propylitic alteration, nearly all carbonate occurrences we have documented to date are late-stage minerals in stockwork veins, microscopic veinlets, and disseminations in QSP-altered rock (figs. 6, 9, 10). The carbonates thus predominantly appear to be an integral component of the QSP vein and alteration assemblages. Total carbonate concentrations measured in hand samples from the QSP-propylitic alteration are generally less than 1–2 weight percent (table 2). It is unclear how the distal, late-stage carbonates may relate temporally or genetically to the deeper, late-stage carbonate-fluorite veins that cut molybdenite mineralization and intrusive granites in the Molycorp open pit and underground workings. The late-stage carbonates and fluorite cutting deeper ore zones appear to be somewhat more abundant than the distal carbonates, based on both observations of earlier workers (Martineau and others, 1977) and observations by Molycorp that carbonates comprise as much as 3–5 percent by volume in the Molycorp tailings (B. Walker, Molycorp, written commun., 2003).

Preliminary examination of polished thin sections shows that microscopic blebs of chalcopyrite and pyrrhotite are relatively common in pyrite from most of the sampled scar areas (fig. 9). Microscopic barite also is relatively common and appears to be contemporaneous with the pyrite (fig. 9). Trace amounts of an unusual Ca-, Ce-, La-, Y-, and F-bearing carbonate (synchysite?, $Ca(Ce,La,Nd,Y)(CO_3)_2F$) are readily determined in drill cuttings from drill hole SC-5B using backscattered-electron SEM imaging (fig. 9)—this mineral also appears to be contemporaneous with hydrothermal pyrite. Hydrothermal phosphate minerals also occur in the stockwork quartz-pyrite veins and are also enriched in light rare earth elements.

Preliminary microprobe analyses (Plumlee, Lowers, and Ludington, 2005) indicate that calcite is the predominant carbonate in the QSP alteration. The calcite generally has low levels of Mn (< several weight percent MnO), Fe (< 2 percent FeO), and Mg (< 0.5 percent MgO).

As noted previously, AVIRIS remote sensing (Livo and Clark, 2002) and subsequent field sampling have identified localized occurrences of breccia-associated advanced argillic alteration in two areas north and south of New Mexico Highway

A. Knob north of the ranger station, underlain by breccia pipe with silica and advanced argillic alteration.

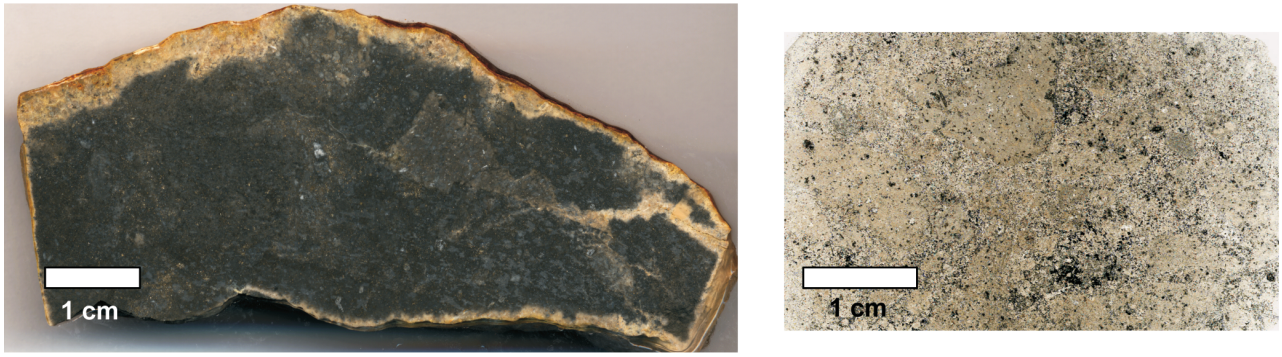

B. Sample Q10-18-02-7, from outcrop in small scar on ridge south of ranger station. Hand sample on left shows bleached rims and veins of sericite encroaching on earlier breccia of alunite- (and pyrophyllite-?) altered clasts. In transmitted light thin section (right) abundant black pyrite is seen in both the breccia matrix and clasts.

C. Sample Q02-22, from outcrop of breccia pipe on Molycorp mine site near ventilation air shaft. Hand sample photo shows hydrothermal breccia with clasts highly altered to pyrophyllite. Matrix contains a mix of pyrophyllite and silica.

Figure 11. Photographs showing occurrences of advanced argillic alteration associated with breccias, lower Red River valley.

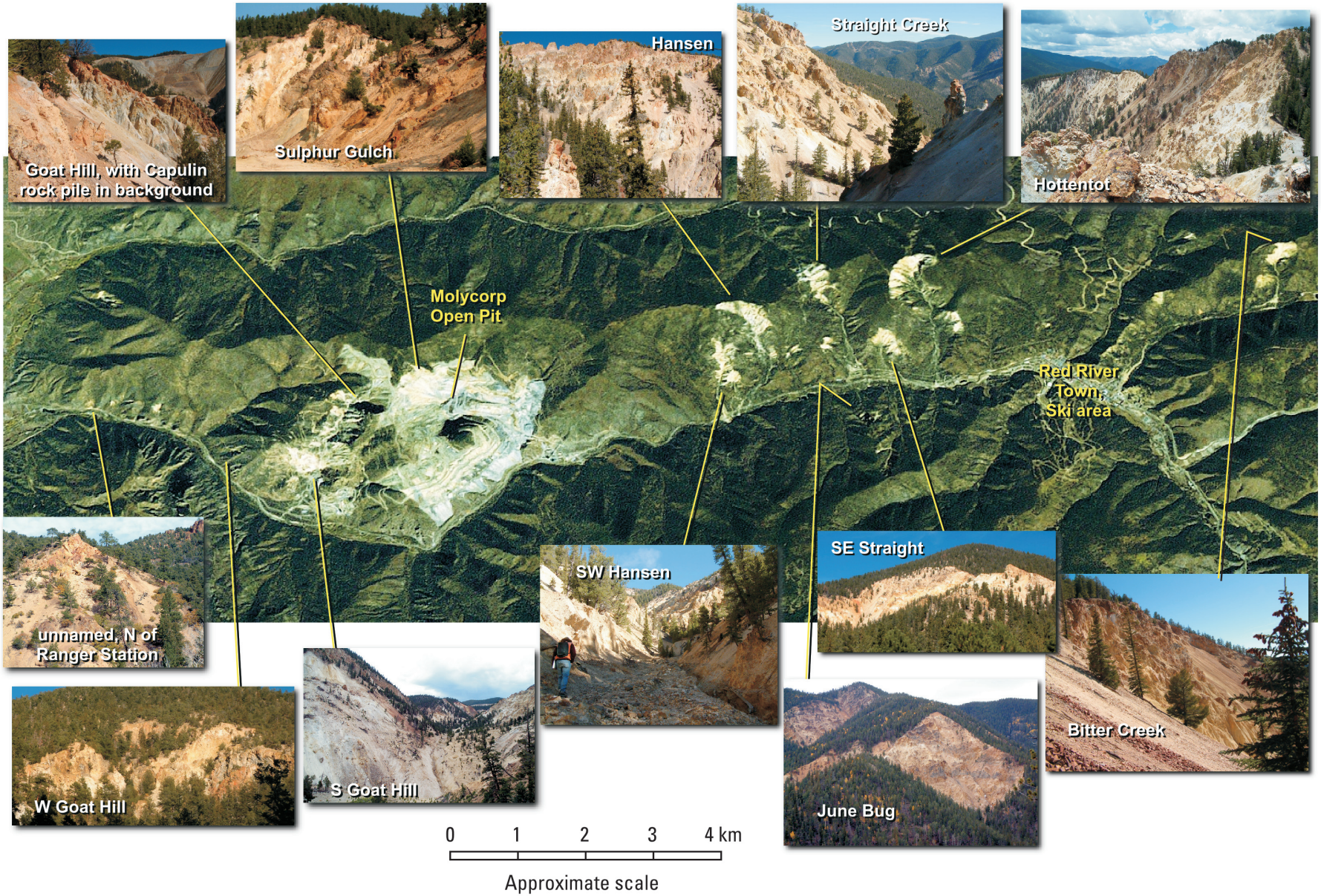

Figure 12. Satellite image (background, from IntraSearch) of the lower Red River showing scar areas, Molycorp mine site, and the town of Red River. Photos of some scar areas are superimposed on the satellite image.

38 near the Red River ranger station and on the hillside southwest of the open pit (fig. 11). These occurrences are marked by alteration of breccia clasts to a mix of pyrophyllite, kaolinite, and (or) alunite (fig. 11). The occurrence south of the ranger station also contains as much as 20 percent by volume pyrite in the breccia matrix. It is unknown how or if these breccia-related occurrences of advanced argillic alteration are related genetically to the molybdenum mineralization.

The Sulphur Gulch scar is the only scar in which erosion was sufficiently deep to expose the mineralization-related granites, the potassic alteration zone, and high-grade molybdenite and ferrimolybdite veins. Descriptions of these rocks, now consumed by the open pit, are not detailed. However, descriptions of the Sulphur Gulch area by Carpenter (1968) and Schilling (1956) prior to open-pit mining suggest that veins of hydrothermal molybdenite, manganiferous carbonates, and fluorite present in the granites near the ground surface were oxidized and leached by descending acid waters, leaving behind secondary ferrimolybdite in veins and disseminations within the uppermost several meters of rock. No potassic alteration is exposed at the surface in any of the other scar areas; however, Loucks and others (1977) note some possible potassic alteration present in deep drill holes in the Straight, Hansen, and Hottentot scars. However, in our reconnaissance survey of drill core from the QE-5 (beneath Sawmill Mountain) and Straight Creek 1 (SC-1) exploration drill holes, we did not observe significant quantities of potassic alteration.

We observed abundant magnetite-hematite stockwork veining in rocks exposed in the upper portions of the Mallette Creek scar. Limited occurrences of magnetite are also noted by Loucks and others (1977) in exploration drill core from depth beneath the Hansen, Straight, and Hottentot scar areas.

Variable Erosion Levels within Mineralized Intrusive Centers along the Lower Red River

Based on the observations presented in the previous sections, it is possible to develop schematic erosional profiles showing the relative depths to which the scar areas have eroded into the hydrothermal alteration zoning patterns developed around the various mineralized intrusive centers along the lower Red River (fig. 6*C*).

The larger western scar areas (Sulphur Gulch, Goat Hill Gulch) have cut deeply into the alteration sequences. The Sulphur Gulch scar cut through QSP-altered andesites and Amalia Tuff (which still remain in its uppermost reaches) and exposed high-grade molybdenite mineralization and potassically altered granitic intrusive rocks in its lower reaches. The Goat Hill Gulch scars cut primarily through intensely QSP altered Amalia Tuff, rhyolite porphyry, and andesites. All of the QSP-altered and propylitically altered Amalia Tuff and andesites have been removed from above the Bear Canyon pluton (fig. 1), leaving behind only granitic rocks with associated molybdenite mineralization.

In contrast, the eastern scar areas (SW. Hansen, Hansen, Straight, SE. Straight, June Bug, Hottentot, SE. Hottentot, Bitter Creek) have generally eroded into the upper or more distal portions of the alteration zoning sequence (fig. 6*C*). These scars have exposed QSP-altered and propylitically altered andesites and quartz latite porphyries, and QS- or advanced argillically altered Amalia Tuff and rhyolite porphyries. The lone exception of the eastern scars is the Mallette scar, which appears to have eroded more deeply through the QSP alteration into magnetite-hematite stockwork. By analogy with the western scars, it can be inferred that granitic intrusive rocks with associated potassic alteration and some molybdenite mineralization of unknown grade should be present at depth beneath one or more of the eastern scars; limited indications of such mineralization were encountered by exploration drilling (Loucks and others, 1977).

Oxidation, Weathering, and Erosion Processes Active in Scars

Meyer and Leonardson (1990) provided the first interpretation that the Red River scars are not primary mineralization features; rather, they resulted from sulfide oxidation, acid weathering, and erosion of the altered rock. Results of this study confirm and add further details to their model.

The alteration scars are characterized by steep, denuded slopes (fig. 12) composed primarily of highly weathered and oxidized rock material. Gullies incised into the denuded slopes typically cut down to unweathered QSP-altered bedrock (figs. 8*B*, 12, 13); such unoxidized bedrock can be found in gully bottoms, even in the higher elevations of the scars to within a few tens of meters of the high ridge crests above the Red River. This suggests that the highly weathered material found in the alteration scars is generally a relatively thin veneer over the QSP-altered bedrock.

Mineralogic Variations in a Weathered Profile Developed on QSP-Altered and Propylitically Altered Andesite

Detailed mineralogical characterization of samples collected from a 2-m-high weathering profile in the Straight Creek scar (fig. 13) provides important insights into oxidation and weathering processes in the scars. Bedrock exposed in the creek bottom is essentially unoxidized and unweathered and is marked by stockwork veins in andesite that have been affected by propylitic and QSP alteration. This rock is extremely hard (resistant to breaking with a hammer) and is physically competent due to extensive silicification. Within a foot above the creek bottom, veinlets of secondary gypsum and iron oxides appear along the stockwork fracture surfaces. Within increasing elevation in the profile, the rock appears to have been increasingly broken apart into progressively smaller polygonal

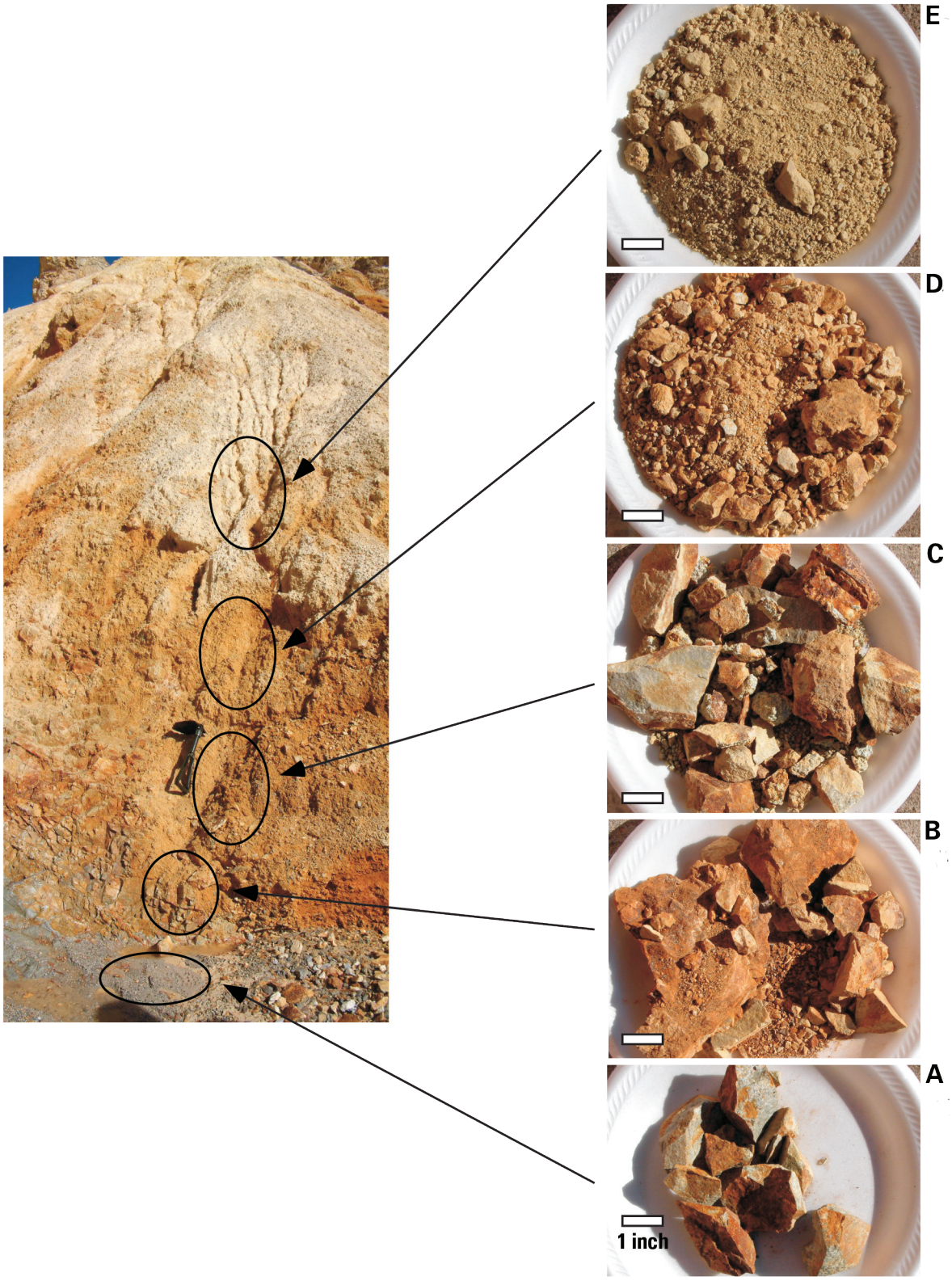

Figure 13. Photograph at left shows weathering profile developed on QSP-altered and propylitically altered andesite, Straight Creek scar. Due to the steepness of topography in the scar, continuous profiles that are not interrupted by shear-failure planes are rare in the scar area. This profile was one of the least disrupted by shear planes. A sequence of samples, Q10-17-02-1A through 1E, was collected at progressively higher elevations in the profile. Photographs on right show bulk samples as collected (plates are 9 inches in diameter). Black circles on left-hand photograph show approximate locations from which corresponding samples were collected.

Table 3. X-ray diffraction results on bulk samples and the <2-mm fraction of samples collected from progressively higher elevations in a weathering profile, Straight Creek scar area.

[Gypsum that was originally present in the rock but that was dehydrated during milling with methanol is noted as bassanite. Smectite is also detected in the bulk samples, from trace levels in samples 1a and 1b to as much as approximately10 weight percent in sample 1e. Smectite values are not included in the table due to a larger analytical uncertainty than achieved for other minerals. Quantitative mineralogy was determined using X-ray diffreaction (XRD). Samples were prepared by adding 10 percent (mass basis) ZnO, which was used to normalize X-ray diffraction patterns. A selected suite of standard minerals was then fit to the sample pattern by least squared-difference, using RockJock, a macro-driven program written for Excel (Eberl, 2003). *, mineral identified quantitatively by XRD but present below significant quantitative percentage (<0.5 percent). Leaders (--) indicate mineral not included in calculated model]

	Q10-17-02-1a	Q10-17-02-1b	Q10-17-02-1c	Q10-17-02-1d	Q10-17-02-1e	Q10-17-02-1b (<2 mm)	Q10-17-02-1c (<2 mm)	Q10-17-02-1d (<2 mm)	Q10-17-02-1e (<2 mm)
Mineral	Weight %	Weight %	Weight %	Weight %	Weight %	Weight %	Weight %	Weight %	Weight %
Quartz	36.1	39.4	35.9	33.8	34.8	17.5	26.9	33.8	31.2
Albite feldspar	12.2	5.3	13.9	11.1	10.4	3.4	10.8	4.1	11.8
Andesine feldspar	2.3	1.5	3.5	3.1	1.9	--	5.8	4.9	--
Plagioclase total	14.5	6.8	17.4	14.1	12.4	3.4	16.6	9.0	11.8
Rutile	0.5	--	--	0.7	0.7	0.9	0.4	--	--
Calcite	0.1	2.9	*	0.6	--	--	--	--	--
Pyrite	2.8	4.8	2.2	1.3	--	22.3	--	--	--
1M illite	9.7	5.1	6.5	7.0	7.3	9.8	10.6	7.7	7.7
2M1 illite	15.2	25.2	15.2	18.2	18.0	20.1	17.7	19.0	20.5
Illite total	24.8	30.3	21.7	25.2	25.3	29.9	28.3	26.7	28.1
Chlorite CO	16.0	--	14.5	--	3.7	5.9	13.8	*	--
Chlorite Tusc	2.2	5.7	4.4	5.4	3.9	--	11.7	12.0	16.5
Chlorite A	5.2	7.6	1.5	12.3	5.8	7.2	2.6	12.9	7.3
Chlorite total	23.4	13.3	20.5	17.7	13.4	13.1	28.1	25.1	23.8
Bassanite	--	1.8	1.1	2.5	1.7	2.8	0.6	0.5	1.5
Jarosite	--	--	0.9	1.7	8.5	2.7	3.5	4.8	11.2
Goethite	0.5	--	--	0.9	0.7	1.8	0.9	1.8	--
TOTAL	**102.9**	**99.2**	**99.7**	**98.5**	**97.6**	**94.4**	**105.4**	**101.7**	**107.7**

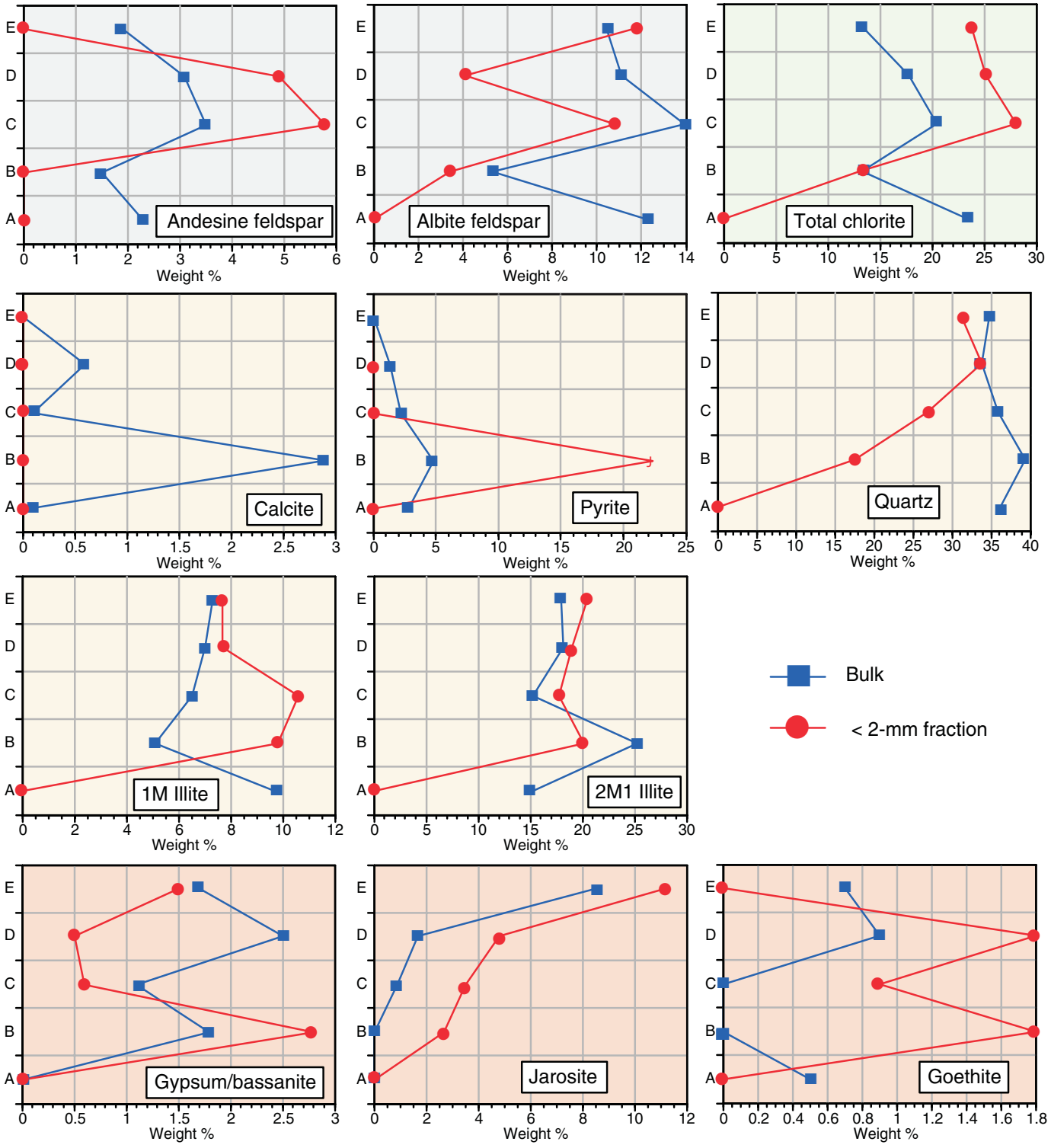

Figure 14. Plots showing variations in the amounts of minerals across the Straight Creek scar weathering profile shown in figure 13. A (letters along vertical axis), unweathered; E, most weathered. Data from table 3. Plots for rock-forming minerals shown with gray background, propylitic alteration minerals with green, predominantly QSP alteration minerals with yellow, and weathering minerals with light orange. Some calcite may be propylitic and some 1M illite may include a smectite component resulting from weathering. Even though it is more weathered, sample B has substantially higher quartz, pyrite, and 2M1 illite (a higher temperature illite) than sample A—this probably reflects a zone of more intense QSP alteration within the bedrock than sample A. Note scale differences in the x axis between different plots.

blocks, primarily along progressively thinner stockwork fractures. At the top of the profile, the weathered material appears in the field and hand samples to be composed of pebble-sized and smaller fragments of unoxidized rock in a matrix of clays and secondary minerals such as jarosite and gypsum.

Quantitative XRD mineralogical analyses of bulk samples from this weathering profile (table 3; figs. 13 and 14) reveal progressive changes in mineralogy resulting from weathering that have been superimposed on variations in the primary alteration mineralogy. Variations in the primary alteration mineralogy are apparent between samples A (unweathered; fig 14), and B (minimally weathered; fig 14) in the profile. Sample B contains greater proportions of pyrite, 2M1 illite (a higher temperature illite than 1M illite), quartz, and calcite, but lesser amounts of feldspar and chlorites than sample A; this suggests that sample B contains a greater proportion of QSP alteration relative to propylitic alteration than sample A. Other bulk mineralogy variations through the profile likely resulted from weathering processes. These include decreases in the pyrite, calcite, and chlorite contents of the bulk rock with increasing elevation in the profile coupled with increases in jarosite and gypsum. Although not quantified in table 3, bulk XRD results suggest that smectite (seen as an increasing smectite component in the illites quantified in table 2) also increases with increasing elevation in the profile, ranging from trace amounts in the unoxidized bedrock at the base of the profile to as much as 10 weight percent in the most weathered material at the top of the profile. Bulk quartz, albite, and illite contents show no consistent trends with elevation. The XRD data suggest that calcic plagioclase (andesine feldspar) may decrease somewhat in amount with increasing elevation in the upper portions of the profile.

Quantitative XRD mineralogical analyses of the fine (< 2 mm) fraction of the upper four samples from this weathering profile (there was no fine fraction of the least weathered sample) indicate that pyrite initially increases in the fine fraction (sample B) and then disappears from all of the more weathered samples. Calcite is not present at all in the fine fraction. With increasing elevation in the profile, goethite increases in abundance in the fine fraction initially, but then decreases in amount until it disappears from the most weathered sample (E; fig 14). Jarosite shows a marked and continuous increase in abundance in the fine fraction with increasing elevation in the profile. Chlorite and illite appear to be preferentially concentrated in the fine fraction relative to the bulk in the most weathered portions of the profile. Sodic plagioclase (albite feldspar) and quartz generally increase in amount in the fine fraction with increasing elevation, whereas more Ca-rich plagioclase (andesine feldspar) initially increases in amount and then decreases substantially in amount in the most weathered sample.

Chemical and Physical Weathering Mechanisms in Rocks Affected by QSP Alteration

The observed mineralogical variations within the Straight Creek weathering profile are consistent with acid weathering of QSP-altered bedrock triggered by sulfide oxidation and the formation of acid-rock drainage (Nordstrom and Alpers, 1999) coupled with physical weathering. Physical breakup of the rock appears to occur along progressively smaller pyrite- and carbonate-bearing veins and fractures with increasing elevation in the weathering profile. Initially, pyrite oxidation and resulting acid chemical weathering of the surrounding material likely causes adjacent pyrite to become more friable, thereby allowing increased access of water into the veins and liberating fine-grained pyrite for further weathering. Freeze-thaw action in the near-surface fractures during the winter may enhance breakup of the rock. Continued pyrite oxidation and chemical weathering effectively removes pyrite and carbonates from the rock fractures and appears to preferentially attack chlorites from among the silicates, possibly converting a small portion of the chlorite to smectitic clays. Increasing quartz, chlorite, illite, and albite proportions in the fine fraction relative to bulk with increasing elevation in the profile suggest that these minerals are preferentially liberated by physical weathering into the fine fraction of the weathered material. The decrease in calcic plagioclase in the bulk and fine fraction in the most weathered sample may indicate that calcic plagioclase is breaking down chemically, again perhaps to smectitic clays. The bulk quartz, sodic feldspars, and illites in the bedrock seem largely unaffected by acid weathering and can be found in abundance in sand- to pebble-size fragments in the most weathered portions of the profile. Secondary gypsum, goethite, and jarosite are precipitated in fractures within the partially weathered rock and (particularly jarosite) make up a substantial part of the matrix of the most weathered rock. Gypsum, jarosite, and other minor soluble salts likely form by evaporation of acid waters during dry periods and help cement the highly weathered material. Gypsum replacement of calcite and pyrite in fractures may also enhance the physical breakup of the rock due to gypsum's substantially greater molar volume.

Weathering and Erosion of Amalia Tuff Altered to Advanced Argillic Assemblages

Amalia Tuff that is distal to the mineralizing intrusions contains pyrite-poor advanced argillic alteration rather than QSP alteration assemblages. Because the advanced argillic assemblages are not pervasive in the rock, and because the negligible pyrite content precludes acid-sulfate weathering, the Amalia Tuff that is distal to mineralizing intrusions is therefore fairly resistant to erosion. Such Amalia caps ridges north of the Red River. It characteristically develops a thin surface coating of bright red hematite on its weathering surfaces and remains

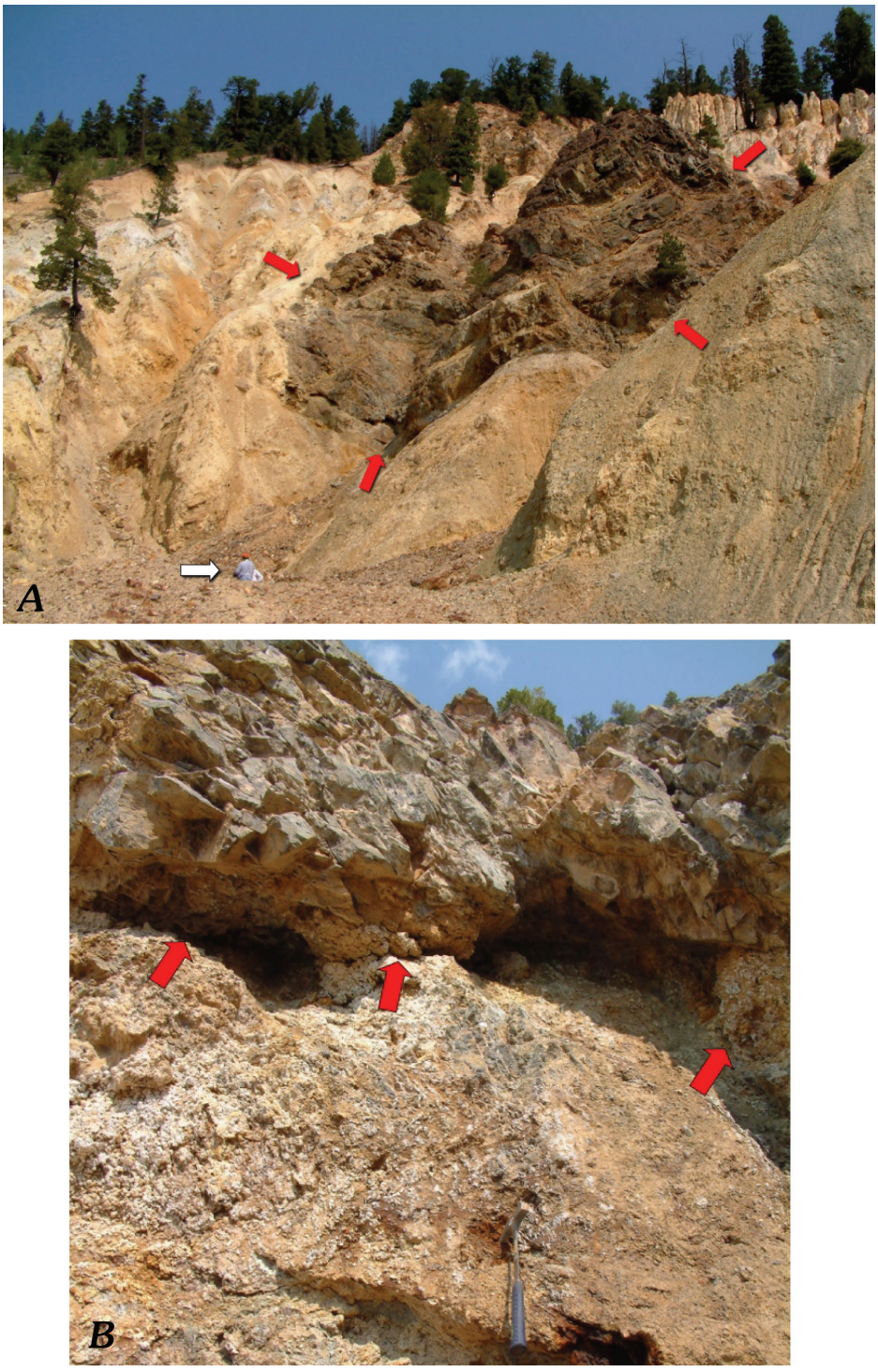

Figure 15. *A*, photograph of house-size slump block of propylitized andesite (dark brown, marked by red arrows) sitting in shear contact on top of weathered, QSP-altered andesite within upper portions of the Sulphur Gulch scar. For scale, white arrow points to man standing on uppermost bench of Molycorp open pit. *B*, closeup photograph of shear contact (red arrows) between slump block and underlying weathered material. Note relatively unweathered appearance of propylitized slump block and presence of abundant white evaporative salts such as gypsum that formed by evaporation of acid waters emanating at the shear contact. Rock hammer is at bottom of photo for scale.

an unweathered gray in its interior. Rather than breaking down chemically, this type of altered Amalia Tuff appears to erode primarily by physical breakup of the rock along clay veins and (or) along pervasive flow-banding surfaces and intersecting vertical joints.

Relative Weathering Rates of Various Rock-Forming, Alteration, and Vein Minerals

The weathering profile provides a good indication of which rock-forming minerals and hypogene vein and alteration minerals in the QSP-propylitically altered rocks are likely to be most chemically reactive when in contact with ground waters in the Red River area. Based on the information from the weathering profile, coupled with information from elsewhere in the literature (i.e., Plumlee, 1999, and references therein) about the weathering rates of minerals not examined in this particular profile, we have developed a general sequence of reactivity for alteration and rock-forming minerals found in the scar areas and mineral deposits along the lower Red River. Minerals listed first in the following sequence have the greatest reactivities are therefore likely to weather more rapidly in the near-surface environment than minerals listed later in the list.

pyrrhotite, pyrite, Ca-carbonate >
chalcopyrite, fluorite, Mn-carbonate, dolomite >
chlorite, epidote? >
calcic plagioclase?, molybdenite? >
illite, biotite?, alunite, kaolinite>
quartz, sodic plagioclase, potassium feldspar

Electron microprobe analyses (Plumlee, Lowers, and Ludington, 2005) of the diverse hydrothermal, alteration, and rock-forming minerals from the various scar areas will help elucidate further the original mineralogic residences for cations, anions, and trace elements measured in ground and surface waters draining the scar areas. Such information can also be used to help further constrain the relative weathering rates and contributions of different minerals to ground-water quality.

Physical Slumping, Erosion Processes, and the Role of Soluble Secondary Salts

Physical and chemical weathering in the scar areas transforms originally competent, resistant rocks into relatively incompetent weathered material that is prone to landslides, slumping, and failure along slip surfaces. As noted by Meyer and Leonardson (1990), the scars likely grow at their steep headwalls by such slumping. Multiple shear planes are readily apparent in weathered material in the steeper portions of the scars. Large slump blocks of less weathered material are common in all of the alteration scars. For example, slump blocks of pyrite-poor propylitized andesite that somehow escaped intense QSP alteration can be seen in many of the scars, sitting in shear contact unconformably on top of highly weathered QSP-altered andesite (fig. 15). The advanced argillically altered Amalia Tuff capping the ridges of the Hansen, Straight, and Hottentot scar areas acts as a more competent unit, forming large slump blocks with steep, jagged cliff faces on the scar slopes. For example, most of the steep SW.-facing slope of the Hansen scar appears to be—when observed from a safe distance—composed primarily of a series of slump blocks of Amalia Tuff (see Hansen scar photo in fig. 12). As also noted by Shaw and others (2003), smaller, isolated Amalia blocks form spires and hoodoos on top of the more weathered andesites. We present further detailed interpretations of possible failure mechanisms in the scar headwalls in a separate paper (Plumlee, Ludington, and others, 2005).

Whereas clays, soluble evaporative salts (such as gypsum), and small rock fragments making up the most weathered rocks in the alteration scars (fig. 13) might seem to be highly vulnerable and prone to rapid physical erosion during intense storm events, our recent observations suggest this may not be the case. As noted in Plumlee, Ludington, and others (2005), gypsum and other soluble salts strongly cement the weathered material and seem to dissolve slowly enough to preclude rapid physical erosion during short-lived thunderstorms. The storms flush loose, rubbly material from the scar gullies during high-flow conditions but do not replenish this loose material as their flow wanes. This indicates that long periods of gentle rainfall or snowmelt (possibly followed by high rainfall) seem to be required to allow sufficient dissolution of salt cement from weathered material to facilitate the transport of the resulting loose, weathered material into the gully bottoms, ready to be flushed again during heavy-runoff events.

Characteristics of Materials in Debris Fans at the Base of Scar Areas

Material eroded from the scars during periods of heavy runoff has accumulated in large alluvial fans at the base of most the scars (see fig. 2). These debris aprons consist of poorly sorted material that ranges in size from large blocks with dimensions of several meters, down to silt- and clay-sized material (Plumlee, Ludington, and others, 2005). Limited mineralogical studies of material in the debris fans shows that it is, as would be expected, a mixture of both relatively unweathered, pyrite-rich mineralized rock and finer grained, weathered material derived from the scar area upstream. Limited XRD analyses of material from the Straight Creek debris fan in the SC-5 drill hole suggest that carbonate minerals are less abundant in the debris-fan material than in unweathered rocks; this lower abundance is consistent with partial leaching of readily accessible carbonates (i.e., those present on grain surfaces or within small fractures in rock fragments) from the weathered material by acid waters, either in the scar areas prior to transport or while in the debris fan.

The debris-fan aprons reach the banks of the Red River and cause the river channel to shift against the opposite wall

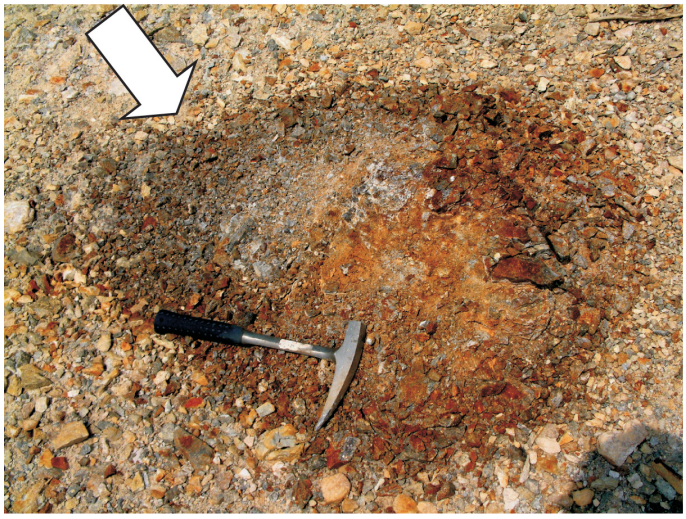

Figure 16. Views of decomposing pyrite-rich rock (marked by white arrows) on debris fan extending from upper Sulphur Gulch scar onto uppermost bench of Molycorp open pit. The rock itself is breaking apart along fractures, and material that has already been eroded from the rock forms a halo around it. Even though we cannot say with certainty that some of the rock breakup did not occur prior to its deposition on the mine bench, geometry of the decrepitated pieces indicates that, at the time the rock was deposited on the bench, it had a distinctly greater cohesion than now.

of the valley. Substantial amounts of fine-grained, altered and mineralized clastic material derived from the scars, as well as acidic, metal-bearing runoff waters, are transported to the river during infrequent periods of high runoff (Robertson GeoConsultants, 2001; Shaw and others, 2003)

How Fast Do Mineralized Rocks in Scars Weather and Degrade?

Without further studies, it is difficult to accurately constrain the time scale during which weathering profiles develop in scar areas. However, a possible indication that the chemical and physical breakup of QSP-propylitically altered rocks may progress fairly rapidly over relatively short time scales (decades?) is provided by a pyrite-rich rock on a debris fan extending from the Sulphur Gulch scar onto the uppermost bench of the Molycorp open pit (fig. 16). We infer that the rock was transported by a debris flow from the scar onto the mine bench sometime after the beginning of open-pit mining in the 1960s and that the rock has decomposed physically and chemically after being deposited on the bench.

Rapid rates of weathering and erosion are also indicated by the large volumes of loose material that are transported by storms from scar areas onto the debris fans. Similarly large volumes of weathered material must also be generated continuously to replenish material removed to the debris fans. A useful future study would be to place more quantitative constraints on the amounts of material transported out of each of the scar areas over the course of several years.

Influences of Hydrothermal Mineralization-Alteration and Secondary Weathering on Ground- and Surface-Water Quality in the Red River Watershed

From an environmental standpoint, mineralogical-characterization studies provide several insights into the roles that mineralization, alteration, and weathering processes in the scar areas play in ground- and surface-water chemistry along the Red River.

Calcite and other carbonates are present in low but variable amounts (as high as several weight percent) in mineralized bedrock beneath the scar areas and their associated debris fans. However, the carbonates are not abundant enough to effectively neutralize the acid generated by intense pyrite oxidation under oxygenated conditions near the ground surface. Readily

accessible carbonates (i.e., those in hydraulically conductive fractures or at grain surfaces) appear to have been effectively leached from the weathered veneer and from underlying shallow bedrock fractures by infiltrating rainfall and snowmelt that had been acidified by sulfide oxidation and dissolution of acid-generating soluble salts.

Waters encountered by the USGS drill holes in the Straight Creek debris fan alluvium are acidic and metal bearing, consistent with the prior removal of readily accessible carbonates from the alluvial material. Such removal may have occurred partly while the material was still present in the scars upstream and partly by the actions of acid waters in the alluvium. In contrast, waters from the bedrock aquifer in the USGS Straight Creek drill holes are near-neutral pH (Naus and others, 2004). The near-neutral pH indicates that carbonate minerals (and, to a lesser extent, more reactive silicates such as chlorite and epidote) in the mineralized bedrock beneath the Straight Creek debris fan are effectively neutralizing acid waters infiltrating from the shallow oxic zones or any acid generated by the limited sulfide oxidation that occurs well below the ground surface out of contact with atmospheric oxygen.

Quite acidic, metal-rich waters emanate from bedrock high in the scar areas, indicating that these waters have undergone extensive sulfide oxidation, salt dissolution, and evaporative concentration, but not acid neutralization. The lack of acid neutralization by carbonates implies that the highly acidic waters are surficial in origin and have interacted primarily with materials in the weathered veneer and shallow bedrock fracture system from which carbonates have been leached. By analogy to ground waters encountered in bedrock in the Straight Creek drill holes, we infer that deeper ground waters beneath the scar areas also have near-neutral pH and correspondingly lower levels of dissolved metals. A schematic section across the lower portions of the Hansen scar (fig. 17) illustrates this interpretation.

The supergene transformation of high-grade molybdenite and carbonate-bearing veins to acid-stable ferrimolybdite- and iron-oxide-rich assemblages in the shallow subsurface of Sulphur Gulch (Carpenter, 1968) indicates that acid waters (perhaps derived from oxidation of pyrite in the Sulphur Gulch scar and pyrite in detrital material from the scar) were infiltrating into the underlying granitic bedrock along veins. These acid waters likely were progressively neutralized by dissolution of carbonates as they flowed into the ground-water system below Sulphur Gulch, eventually ending up with near-neutral pH. Because carbonates in the rocks beneath Sulphur Gulch were manganese rich (Schilling, 1956; Carpenter, 1968; Martineau and others, 1977), it is likely that the ground waters beneath Sulphur Gulch were relatively enriched in manganese content. It interesting to note that the first appearances of manganocrete deposition in the Red River downstream from the town of Red River occur at and below the premining Sulphur Gulch confluence with the Red River.

A potential modern analog for these processes may exist on the Molycorp mine site. Acid-rock drainage collected from mine waste piles on the western side of the mine site is shunted into the surficial subsidence zone above the underground Molycorp workings. The acid-rock drainage percolates into the highly disturbed rocks beneath the subsidence zone. Waters that drain from the subsidence zone into mine workings some 1,000 ft below the surface are near-neutral pH, suggesting that interactions with carbonate minerals may produce significant chemical transformations such as increases in pH.

Geologic Structures and Bedrock Ground-Water Flow System

The previous section illustrates some of the ways that bedrock lithology and hydrothermal mineralization and alteration types may influence ground-water parameters such as pH. This section provides a brief description of significant structural features in the lower Red River watershed and how those structural features may influence ground-water flow through the mineralized bedrock.

The bedrock of the Red River watershed and Questa caldera includes a variety of complex geological structures formed during a long history of volcanic and tectonic activity. In order to characterize the potential geological controls on the bedrock ground-water flow system, field observations and measurements of brittle structures were made at locations representative of each of the major lithologies within the study area (fig. 18 and Caine, 2003). Because the majority of the bedrock in the Questa study area is crystalline, it may be reasonable to assume that its porosity and permeability are controlled by secondary brittle structures such as faults, joint networks, and vein systems.

Potentially the most hydraulically significant geologic structures observed during recent field work are a set of high-angle, extensional faults striking north-south (also see Meyer and Foland, 1991) that are characterized by open, conjugate fracture networks. The intensity of these faults were measured along horizontal traverses at two localities, one in rhyolite dikes at Cabin Springs and one uphill from Cabin Springs in weakly propylitized rock; on average there is approximately one fault every 10 m (J.S. Caine, written commun., 2004). This intensity of faulting may contribute significantly to ground-water flow. The caldera margin is mapped (Lipman and Reed, 1989; Meyer and Leonardson, 1990) as a fault zone that intersects the Red River in several locations. Observations of this fault zone in outcrop exposures indicate extensive fault-related fracturing; however, the hydraulic influence of this structure, conduit or otherwise, has not been determined (J.S. Caine, written commun., 2004).

Joint-network properties measured for all Questa lithologies and hydrothermal alteration types show that joint networks are of high intensity, are highly interconnected, and have multiple orientations with typically small apertures (< 1 mm). Combined, these physical joint-network properties may result in relatively homogeneous hydraulic properties and thus impart nearly isotropic, albeit low, bulk permeability to the flow system at the watershed scale.

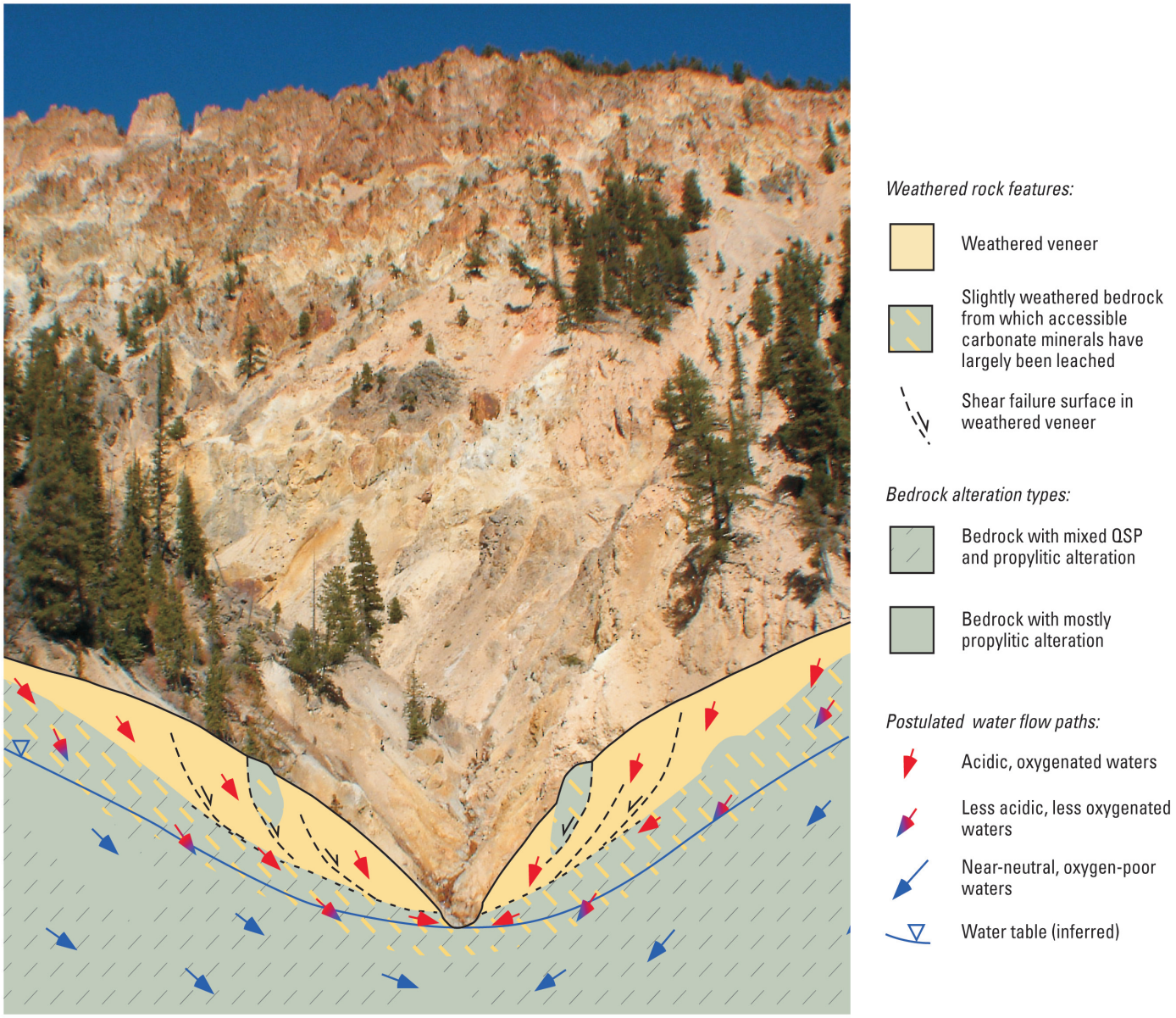

Figure 17. Schematic west-to-east cross section of shallow subsurface at base of a typical scar area superimposed on photograph of the Hansen scar. Illustrated is the inferred nature of weathered veneer of surficial deposits and bedrock, their potential geochemical interactions with ground waters, and potential pathways for transport of acidic waters. Red and blue arrows are not calculated flow paths but show relative geochemical characteristics associated with different geological units and are for illustrative purposes only. Note the red-orange, acidic surface waters flowing along the gully bottom in the photograph. Darker slump blocks of less weathered bedrock (likely a result of localized and less intense QSP alteration and stockwork veining) are readily visible in the lighter yellow to tan weathered veneer in the photograph and are so depicted in the cross section. Due to the steep gradient from the ridge top to the gully bottom, there is likely a significant component of ground-water flow out of the cross section toward the viewer. The steep cliffs in the background appear to be a series of slump blocks of Amalia Tuff overlying highly weathered QSP-altered andesite.

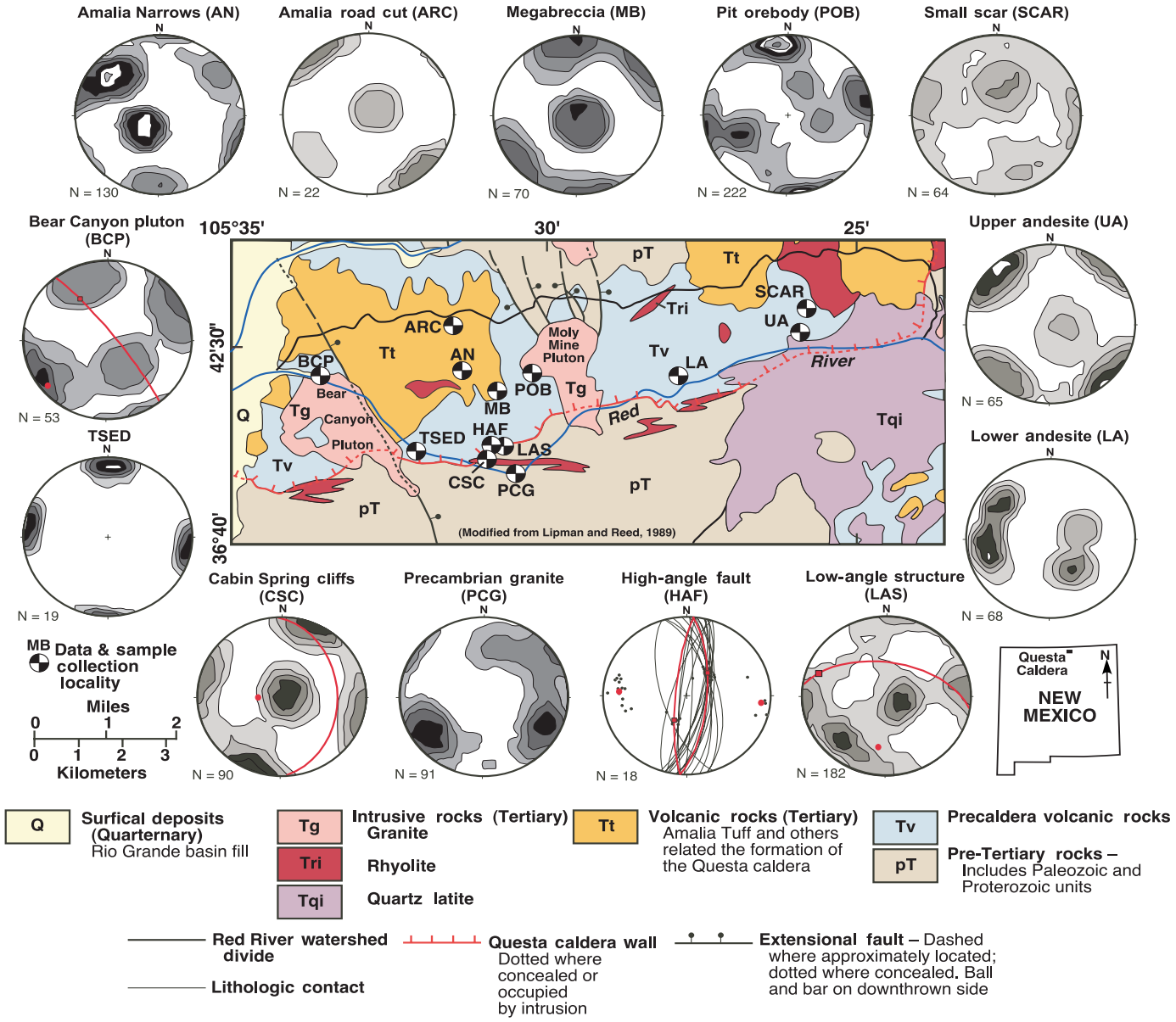

Figure 18. Simplified geologic map of the Questa caldera (modified from Lipman and Reed, 1989). Fracture network and fault-zone data-collection localities are shown (BCP, Bear Canyon pluton; AN, Amalia Narrows; ARC, Amalia road cut; MB, Megabreccia; TSED, Tertiary sediments; HAF, High-angle fault; LAS, Low-angle structure; CSC, Cabin Spring cliff; PCG, Precambrian granites; POB, Pit orebody; LA, Lower andesite; UA, Upper andesite; SCAR, Small scar outcrop). Poles to fractures are shown and contoured on equal-area nets using the Kamb method. All contour intervals are 2 sigma, and N equals the number of fractures measured. Mean great circles for fault-plane orientations and their mean poles are shown in red.

In the near surface, the pervasive and high-intensity nature of open joint networks in the mineralized rocks may provide pathways through which surface waters and ground waters can transport acid and metals liberated by sulfide oxidation and acid-sulfate weathering (fig. 17). Various discrete features—such as open fault zones that cut the joint networks and vein systems—may dominate the flow system in terms of the bulk amounts of ground water they transmit. Additionally, the dominant north-south faults follow the extreme topographic or elevation head gradient (mean ~ 0.3) from the ridge crests in the north to the Red River to the south (fig. 19). Because many of these north-south faults are open and parallel the topographic gradient, it can be inferred that there is potential for significant but highly discrete north-to-south ground-water flow through the mineralized bedrock caused by these structures.

In numerous regions of the world where there is low-permeability, fractured, crystalline bedrock covered by higher permeability, weathered bedrock and surficial deposits, the bedrock is often assumed not to be a major contributor to the transport of ground water (Davis and Turk, 1964). In the lower

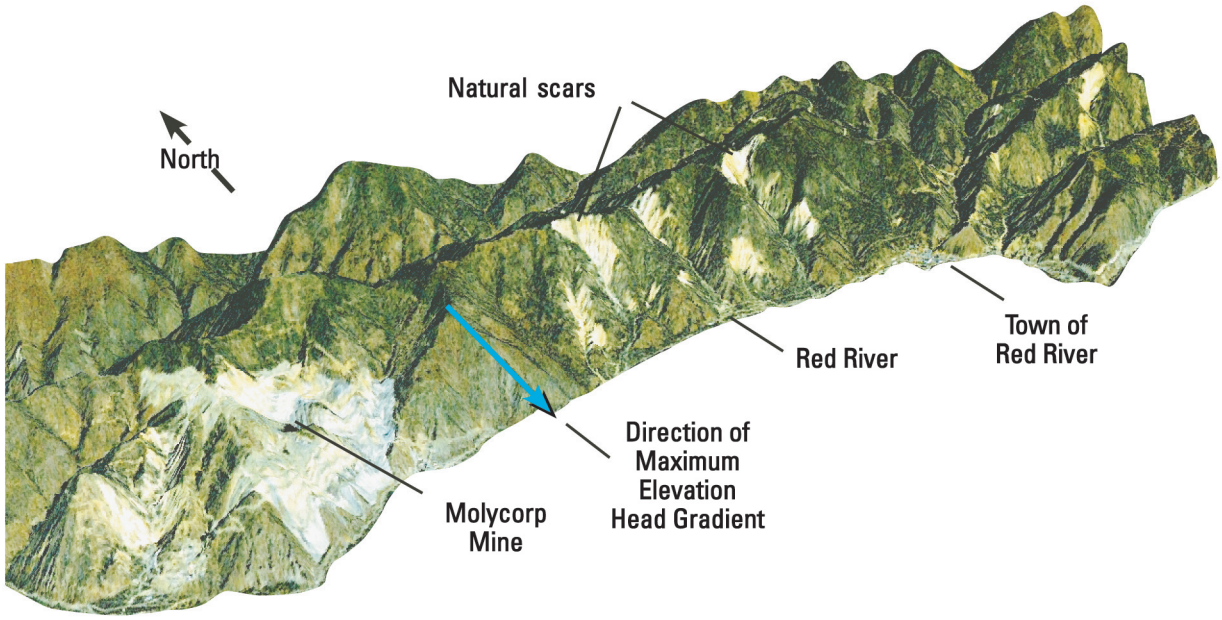

Figure 19. Fifteen-meter natural-color satellite image (from IntraSearch) draped on a USGS digital elevation model (DEM). Topographic and geologic margin of Questa caldera faces the reader. Note extreme topographic gradient (average side canyon relief ~ 660 m) toward the Red River. Many of the high-angle extensional faults observed in the field trend north-south and parallel this gradient.

Red River watershed, the presence of open faults paralleling the topographic gradient may indicate that the bedrock is locally a greater contributor to ground-water flow than is often assumed. Geological observations are not hydraulic reality, and inferences made, such as the ones presented above, must be used with caution. Therefore, geological observation should be integrated with hydraulic testing and time series water-level data to provide constraints on the potential structural impacts on bedrock ground waters as well as bedrock interactions with surficial deposits, and the open pit and underground mine workings after mine closure.

Are Unmined Erosional Scars Good Analogs for Mine-Site Scars under Premining Conditions?

We interpret the altered and weathered rocks that are exposed in the series of scars along the Red River trend to be part of a complex of geologically similar, multistage, mineralized intrusive centers that formed after 25 Ma as cupolas along the roof of a single batholith at depth beneath the trend. The highly evolved granites and porphyries that are uniquely associated with molybdenite mineralization are largely restricted to the trend. Many of these rock units are themselves elongated along the same direction, occurring as dike-like bodies mapped on both sides of the Red River, east and south of the Questa mine area. The mineralogical and geochemical character of the QSP-altered rock in scars that are distant from known mineralization (scars primarily in the eastern part of the trend) is similar to altered rock associated with known mineral deposits in the western part of the trend.

In this section, we will summarize and compare the geological, mineralogical, and weathering characteristics of the unmined scars to those that existed in the similar Sulphur Gulch, Goat Hill Gulch, and Truck Shop scars that formed much of the premining surface above the mined orebodies.

When molybdenite mining began in the Questa area during WWI, Sulphur Gulch and Goat Hill Gulch were erosional scars similar to those presently found in Hottentot, Straight, and Hansen Creeks (fig. 2). Original mining in the lower part of Sulphur Gulch was by traditional stoping methods on individual quartz-fluorite-molybdenite veins. From that area upstream, Sulphur Gulch was apparently an erosional scar developed in QSP-altered rocks. Only the uppermost portions of this scar remain today above the northwest margin of the Molycorp open pit (figs. 15, 16). The largest part of the Sulphur Gulch scar was consumed by open pit during mining from 1965 to the early 1980s. Other parts have been converted to roads or filled for other ancillary development. Two smaller scars were also present, Southeast Truck Shop and South Truck Shop (fig. 2). These scars were covered by waste dumps after 1965 (Meyer and Leonardson, 1990). The Goat Hill Gulch scar has been affected primarily by the addition of several mine-waste piles in its upper reaches, excavation of a network of mine roads, and the development of the mining-related subsidence area near the South Goat Hill scar.

Similarities Between Scar Areas

The scar areas affected by mining were probably similar, prior to mining, to the unmined scars upstream in the following ways:

- The topography in upper Sulphur Gulch and in Goat Hill Gulch prior to mining was similar to that of south-facing, unmined scars. Steep, poorly vegetated slopes in the scars were undergoing rapid physical erosion and chemical leaching, with most mass wasting occurring during seasonal thunderstorms.
- As shown in table 1, many of the unmined scars—and the ones present before 1965 in Sulphur Gulch and Goat Hill Gulch—were approximately the same size and would have provided similar fluxes of detritus into the Red River valley.
- Like the unmined scars, the upper Sulphur Gulch and Goat Hill Gulch scars exposed QSP-altered rocks, with their attendant stockwork veining and elevated pyrite contents, to physical and chemical weathering.
- Like the unmined scars, the upper Sulphur Gulch and Goat Hill Gulch scars are developed on rocks that have undergone extensive fracturing (originally noted by Meyer and Leonardson, 1990). As noted in this study, hydrothermal stockwork fracturing and veining of the bedrock (a feature common to all the scar areas) clearly plays a role in the accelerated chemical weathering and physical breakup of the originally highly competent, silicified QSP rock.
- We observed no difference in the intensity of hydraulically conductive, postmineralization fracturing (such as the open, high-angle N.-S. faulting mentioned in the previous section) between upper Sulphur Gulch and Goat Hill Gulch and the scar areas to the east.
- The geochemical abundances of most metals within the premining upper Sulphur Gulch scar would have been generally similar to those found in the scars to the east today. Perhaps the best direct support for this inference is provided by the geochemical maps presented in Robertson GeoConsultants (2001). The maps for molybdenum, lead, tin, and fluorine demonstrate the presence of these introduced elements in the QSP alteration zones exposed at many places along the length of the N. 75° E. trend, from Bear Canyon to east of Straight Creek (fig. 5).
- All of the scar areas were initiated in the same manner, that is via the coupled chemical weathering, physical breakdown, and subsequent erosion of volcanic rocks containing widespread quartz-pyrite stockwork mineralization and associated quartz-sericite-pyrite alteration.

Differences Between Scar Areas

Some important differences do exist between the mining-affected scars and the unmined scars:

- The Sulphur Gulch scar eroded to substantially deeper levels within its mineralized system than did any of the other scars in the lower Red River watershed (fig. 6). As a result, there was ore-grade molybdenite mineralization present at the surface in the lower reaches of the Sulphur Gulch scar, with molybdenite-bearing, low-pyrite, potassically altered rock composed primarily of quartz, alkali feldspar, and some biotite. In addition, there were significant amounts of late-stage fluorite and carbonates (manganiferous calcite, and iron-rich rhodochrosite and dolomite) in the gangue of veins that were mined. Further, the bedrock in this area was granite and aplite, rather than volcanic rock, and distinctly less iron and magnesium would have been available for dissolution than from the andesites abundant in other scars. In addition, the topographic gradient of lower Sulphur Gulch was considerably flatter than in the lower portions of other scar areas due to the exposure of the less easily eroded granites. All these factors would have helped mitigate the generation of acid-rock drainage, leaching of metals, and the erosion of material from the bedrock in the lower parts of the Sulphur Gulch scar.
- The geochemical maps in Robertson GeoConsultants (2001) indicate that some metals (zinc, copper, and manganese) may have been more abundant in the Sulphur Gulch and Goat Hill Gulch scars than in the Straight Creek, Hottentot, Hansen, and other scars—this is likely a result of the closer proximity of the altered rocks in the Sulphur Gulch and Goat Hill scars to the mineralizing intrusions.
- Inspection of topographic maps compiled prior to open-pit mining indicates that the alluvial fan developed at the base of Sulphur Gulch was not nearly as spatially or volumetrically extensive as fans developed below the other scar areas. Perhaps, due to the location of the Sulphur Gulch outflow at a bend in a narrow portion of the Red River canyon, the alluvial material was rapidly eroded by flow of the Red River. If this is the case, then there would not have been as extensive a volume of potentially acid generating sediments as are present in alluvial fans below the unmined scar areas upstream.
- QSP-altered bedrock is exposed at the ground surface within 30 m or so of the Red River just downstream from the Goat Hill Gulch alluvial fan (outcrops in the road cut at the mine-site entrance), and within 100 m of the river farther downstream near Capulin Canyon. Fractures in this bedrock may provide a conduit for waters draining QSP-altered rocks west of the mine site directly into the river system. In contrast, sulfide-bearing bedrock outcrops are quite distant from the Red River in the upstream south-facing scar areas due to the development of extensive alluvial fans.

Summary

The results and interpretations of this study provide insights into the important roles that bedrock geology, hydrothermal alteration and mineralization, and geologically rapid weathering and mechanical erosion of mineralized rocks play in controlling scar development and ground- and surface-water quality along the lower Red River watershed.

The altered rocks that are exposed in the series of scars along the lower Red River are part of a complex of geologically similar, multistage, mineralized intrusive centers that formed as cupolas along the roof of a single batholith at depth. There are many similarities in intrusive rock types and styles of alteration and mineralization between the various scar areas, suggesting that the intrusive centers were similar in magma chemistry and produced a similar suite of mineralization types, alteration zoning patterns, and trace-element enrichments. The intrusive centers were generally introduced into the same suite of predominantly volcanic and subvolcanic host rocks, although there are some differences in the particular rock types present and (or) their proportions between the various scar areas.

Most importantly, the biggest difference observed between some of the different scar areas is the depth to which erosion has cut into the mineralization/alteration zoning sequence around the intrusions. The deepest levels of erosion are observed in the Bear Canyon pluton west of the Molycorp mine site (where only the molybdenite-mineralized granitic intrusions remain) and the Sulphur Gulch scar on the Molycorp mine site (which exposed an extensive alteration sequence extending from QSP-altered volcanics in its uppermost portions down to molybdenite-mineralized granite intrusion in its lower portions). Nearly all of the other scar areas cut primarily through QSP and more distal QS, propylitic, and advanced argillic alteration.

All of the scar areas were initiated and continue to grow by the same processes involving coupled chemical weathering, physical breakdown, and subsequent erosion of volcanic rocks containing widespread quartz-pyrite stockwork mineralization and associated QSP alteration. Oxidation of pyrite in stockwork fractures generates acidic waters, which in turn chemically weather the surrounding rock, primarily attacking pyrite and other sulfides, carbonates, fluorite, chlorite, epidote, and possibly some illite and calcic plagioclase. The chemical weathering may convert some of the chlorite, illite, and calcic plagioclase to clay minerals such as smectite and kaolinite. Evaporation of the acid waters precipitates gypsum, jarosite, and goethite in the weathered rock. Due to the chemical weathering and physical weathering (such as freeze-thaw action and volume expansion resulting from gypsum precipitation), the rock is broken into progressively smaller polygonal fragments along the stockwork fractures. The physical and chemical weathering observed in the scar areas transforms originally quite competent, resistant rocks into relatively incompetent weathered material that is prone to landsliding and slumping due to its high clay content and generally fine grain size. The weathered material forms a relatively thin (generally 10 to 100 ft thick) veneer throughout the scars, which grow at their headwalls by slumping of the weathered material.

Quite acidic, metal-rich waters develop in the near-surface weathered veneer and shallow bedrock in the scar areas, in spite of the carbonates originally present in the rock. However, there are sufficient carbonates in QSP-altered bedrock to neutralize acid in the deeper ground waters—these tend to have near-neutral pH and lower metal contents. The composition of ground waters in the deeper molybdenite mineralization likely is influenced strongly by interactions with manganiferous carbonates and fluorite present in the abundant late-stage veins.

There are some important differences between the mine site's Sulphur Gulch scar prior to mining and the upstream scar areas. However, their similarities are sufficient to suggest that the upstream scar areas can, with appropriate attention to details of geology and mineralogy, provide useful constraints on premining ground- and surface-water conditions in the mine site scars prior to mining.

References

Caine, J.S., 2003, Questa baseline and pre-mining groundwater quality investigation 6. Preliminary brittle structural geologic data, Questa mining district, southern Sangre de Cristo Mountains, New Mexico: U.S. Geological Survey Open-File Report, OF 03-0280, 24 p., http://pubs.usgs.gov/of/2003/ofr-03-280/.

Carpenter, R.H., 1968, Geology and ore deposits of the Questa molybdenum mine area, Taos County, New Mexico, *in* Ridge, J.D., ed., Ore deposits of the United States, 1933–1967 (Graton-Sales volume): New York, American Institute of Mining. Metallurgical, and Petroleum Engineers, v. 2, p. 1328–1350.

Carten, R.B., White, W.H., and Stein, H.J., 1993, High-grade granite-related molybdenum systems—Classification and origin, *in* Kirkham, R.V., Sinclair, W.D., Thorpe, R.I., and Duke, J.M., eds., Mineral deposit modeling: Geological Association of Canada Special Paper 40, p. 521–554.

Czamanske, G.K., Foland, K.A., Kubacher, F.A., and Allen, J.C., 1990, The $^{40}Ar/^{39}Ar$ chronology of caldera formation, intrusive activity, and Mo-ore deposition near Questa, New Mexico, *in* Bauer, P.W., Lucas, S.G., Mawer, C.K., and McIntosh, W.C., eds., Tectonic development of the southern Sangre de Cristo Mountains, New Mexico: New Mexico Geological Society Guidebook, v. 41, p. 355–358.

Davis, S.N., and Turk, L.J., 1964, Optimum depth of wells in crystalline rocks: Groundwater, v. 2, p. 6–11.

Dillet, B., and Czamanske, G.K., 1987, Aspects of the petrology, mineralogy, and geochemistry of the granitic rocks associated with Questa caldera, northern New Mexico: U.S. Geological Survey Open-File Report 87-258, 238 p.

Gunow, A.J., Ludington, S.D., and Munoz, J.L., 1980, Fluorine in micas from the Henderson molybdenite deposit, Colo.: Economic Geology, v. 75, p. 1127–1137.

Johnson, C.M., and Lipman, P.W., 1988, Origin of metaluminous and alkaline volcanic rocks of the Latir volcanic field, northern Rio Grande rift, New Mexico: Contributions to Mineralogy and Petrology, v. 100, p. 107–128.

Johnson, C.M., Czamanske, G.K., and Lipman, P.W., 1989, Geochemistry of intrusive rocks associated with the Latir volcanic field, New Mexico, and contrasts between evolution of plutonic and volcanic rocks: Contributions to Mineralogy and Petrology, v. 103, p. 90–109.

Jones, D.M., 1990, Mid-Tertiary arcuate dikes and faults of the Rio Hondo–Red River drainages, Sangre de Cristo Mountains, New Mexico; a postulated overlying ring-fracture zone to the Miocene Questa caldera, *in* Bauer, P.W., Lucas, S.G., Mawer, C.K., and McIntosh, W.C., eds., Tectonic development of the southern Sangre de Cristo Mountains, New Mexico: New Mexico Geological Society Guidebook, v. 41, p. 365–368.

Jones, D.M., and Norris, J.R., 1984, Geology of the South Fork molybdenum occurrence, Taos County, New Mexico, *in* Baldridge, W.S., Dickerson, P.W., Riecker, R.E., and Zidek, J., eds., Rio Grande Rift—Northern New Mexico: New Mexico Geological Society Guidebook, v. 35, p. 213–218.

Leonardson, R.W., Dunlop, G., Starquist, V.L., Bratton, G.P., Meyer, J.W., Osborne, L.W., Atkin, S.A., Molling, P.A., Moore, R.F., and Olmore, S.D., 1983, Preliminary geology and molybdenum deposits at Questa, New Mexico: Wheat Ridge, Colo., Proceedings of the Denver Region Exploration Geologists Society Symposium: The genesis of Rocky Mountain ore deposits; changes with time and tectonics, p. 151–156.

Lipman, P.W., 1983, The Miocene Questa caldera, northern New Mexico; relation to batholith emplacement and associated molybdenum mineralization: Wheat Ridge, Colo., Proceedings of the Denver Region Exploration Geologists Society symposium: The genesis of Rocky Mountain ore deposits; changes with time and tectonics, p. 133–147.

Lipman, P.W., 1992, Ash-flow calderas as structural controls of ore deposits—Recent work and future problems, *in* Thorman, C.H., ed., Application of structural geology to mineral and energy resources of the Central and Western United States: U.S. Geological Survey Bulletin 2012, p. L1–L12.

Lipman, P.W., and Reed, J.C., Jr., 1989, Geologic map of the Latir volcanic field and adjacent areas, northern New Mexico: U.S. Geological Survey, Miscellaneous Investigations Map I-1907, scale, 1:48,000.

Livo, K.E., and Clark, R.N., 2002, Mapped minerals at Questa, New Mexico, using airborne visible-infrared imaging spectrometer (AVIRIS) data—Preliminary report for: First quarterly report of the U.S. Geological Survey investigation of baseline and pre-mining ground-water quality in the Red River valley basin, New Mexico, November 13, 2001: U.S. Geological Survey Open-File Report 02-0026, 13 p.

Loucks, T.A., Phillips, J.S., and Newell, R.A., 1977, Exploration potential of the Questa East area, unpublished report for Kennecott Copper Corporation.

Ludington, S.D., 1981, Quartz-pyrite-molybdenite stockwork near South Fork Peak, Taos County, New Mexico: U.S. Geological Survey Open-File Report 81-1080, 10 p.

Ludington, S.D., 1986, Descriptive model of Climax Mo deposits, *in* Cox, D.P., and Singer, D.A., eds., Mineral deposit models: U.S. Geological Survey Bulletin 1693, p. 73.

Ludington, S.D., Bookstrom, A.A., Kamilli, R.J., Walker, B.M., and Klein, D.P., 1995, Climax Mo deposits, *in* du Bray, E.A., ed., Preliminary compilation of descriptive geoenvironmental mineral deposit models: U.S. Geological Survey Open-File Report 95-831, p. 70–74.

Martineau, M.P., Heinemeyer, G.R., Craig, S.D. and McAndrews, K.P., 1977, Geological report, Questa project, 1975–1977, Questa Molybdenum Company, unpublished report, 161 p.

Meyer, J.W., 1991, Volcanic, plutonic, tectonic, and hydrothermal history of the southern Questa caldera, New Mexico: University of California at Santa Barbara, unpub. Ph.D. dissertation, 287 p.

Meyer, J.W., and Foland, K.A., 1991, Magmatic-tectonic interaction during early Rio Grande rift extension at Questa, New Mexico: Geological Society of America Bulletin, v. 103, p. 993–1006.

Meyer, J.W., and Leonardson, R.W., 1990, Tectonic, hydrothermal and geomorphic controls on alteration scar formation near Questa, New Mexico, *in* Bauer, P.W., Lucas, S.G., Mawer, C.K., and McIntosh, W.C., eds., Tectonic development of the southern Sangre de Cristo Mountains, New Mexico, New Mexico Geological Society Guidebook, v. 41, p. 417–422.

Molling, P.A., 1989, Applications of the reaction progress variable to the hydrothermal alteration associated with the deposition of the Questa molybdenite deposit, NM: Johns Hopkins University, unpub. Ph.D. dissertation, 229 p.

Mutschler, F.E., Wright, E.G., Ludington, S.D., and Abbott, J.T., 1981, Granite molybdenite systems: Economic Geology, v. 76, p. 874–897.

Naus, C.A., McCleskey, R.B., Donohoe, L.C., Nordstrom, D.K., Paillet, F.L., and Verplanck, P.L., 2004, Questa baseline and pre-mining ground-water quality investigation. 5. Well installation, water-level data, and surface- and ground-water chemistry in the Straight Creek Drainage Basin, Red River Valley, New Mexico, 2001–2003: U.S. Geological Survey Open-File Report 2005-5088.

Nordstrom, D.K., and Alpers, C.N., 1999, Geochemistry of acid mine waters, *in* Plumlee, G.S., and Logsdon, M.J., eds., The environmental geochemistry of mineral deposits, Part A: Processes, techniques, and health issues: Society of Economic Geologists, Reviews in Economic Geology, v. 6A, p. 133–160.

Plumlee, G.S., 1999, The environmental geology of mineral deposits, *in* Plumlee, G.S., and Logsdon, M.J., eds., The environmental geochemistry of mineral deposits, Part A: Processes, techniques, and health issues: Society of Economic Geologists, Reviews in Economic Geology, v. 6A, p. 71–116.

Plumlee, G.S., Lowers, H., Ludington, S., 2005, Questa baseline and pre-mining ground-water quality investigation. 14. The chemical composition of bulk rocks and minerals from mined and unmined porphyry molybdenum mineralization along the Red River, New Mexico: Implications for ground- and surface-water quality. U.S. Geological Survey Open-File Report.

Plumlee, G.S., Ludington, S., Vincent, K.R., Verplanck, P.L., Caine, J.S., and Livo, K.E., 2005, Questa baseline and pre-mining ground-water quality investigation, 8. A photographic record of chemical weathering, erosional processes, and potential debris-flow hazards in scar areas developed on hydrothermally altered rocks; U.S. Geological Survey Scientific Investigations Report.

Robertson GeoConsultants, Inc., 2001, Background study data report, Questa mine, New Mexico: Vancouver, B.C., Robertson GeoConsultants, 40 p., 58 figures, 10 tables, 20 photographs, 2 oversize maps, 1 CD-ROM.

Ross, P., Jébrak, M., and Walker, B.M., 2002, Discharge of hydrothermal fluids from a magma chamber and concomitant formation of a stratified breccia zone at the Questa porphyry molybdenum deposit, New Mexico: Economic Geology, v. 97, p. 1679–1700.

Schilling, J., 1956, Geology of the Questa molybdenum (Moly) mine area, Taos County, New Mexico: New Mexico Bureau of Mines and Mineral Resources Bulletin 51, 87 p.

Shaw, S., Wels, C., Robertson, A., Fortin, S., and Walker, B., 2003, Background characterization study of naturally occurring acid-rock drainage in the Sangre de Cristo Mountains, Taos County, New Mexico: Proceedings, 6th International Conference on Acid-Rock Drainage (ICARD), p. 605–616.

Smith, K.S., Hageman, P.L. Briggs, P.H., Sutley, S.J., McCleskey, R.B., Livo, K.E., Verplanck, P.L., Lamothe, P.J., and Gemery, P.A., 2005, Questa baseline and pre-mining ground-water quality investigation, 19. Bulk chemistry, mineralogy, and leaching characteristics of mine-waste materials and naturally weathered areas near Questa, New Mexico: U.S. Geological Survey Open-File Report.

Westra, G., and Keith, S.B., 1981, Classification and genesis of stockwork molybdenum deposits: Economic Geology, v. 76, p. 844–873.

Published in the Central Region, Denver, Colorado
Manuscript approved for publication November 2, 2004
Edited by Richard W. Scott, Jr.
Graphics by the authors